AD-A092 690 HUGHES RESEARCH LABS MALIBU CA F/6 20/6
OPTICAL MICROWAVE INTERACTIONS IN SEMICONDUCTOR DEVICES.(U)
NOV 80 L FIGUEROA, C W SLAYMAN, H W YEN N00173-78-C-0192
UNCLASSIFIED NL

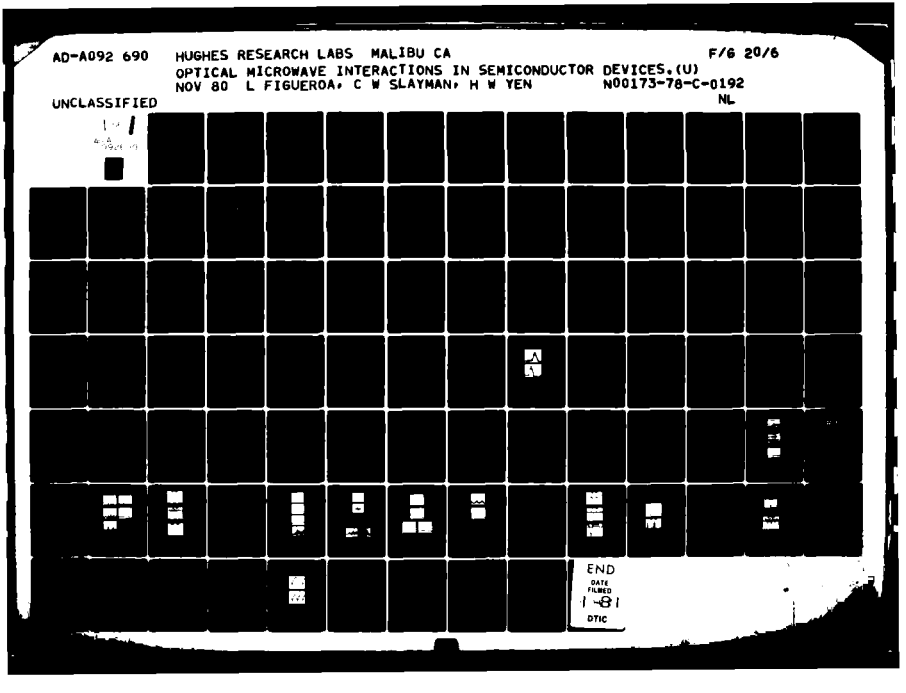

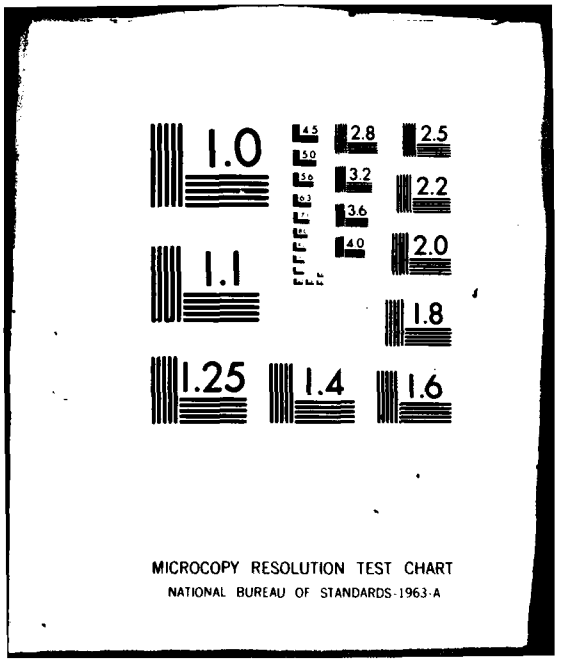
1.0
1.1
1.25
1.4
1.6
1.8
2.0
2.2
2.5
2.8
3.2
3.6
4.0
4.5
5.0
5.6
6.3
MICROCOPY RESOLUTION TEST CHART
NATIONAL BUREAU OF STANDARDS-1963-A

OPTICAL MICROWAVE INTERACTIONS IN SEMICONDUCTOR DEVICES

L. Figueroa, C.W. Slayman, and H.W. Yen

Hughes Research Laboratories
3011 Malibu Canyon Road
Malibu, CA 90265

November 1980

N00173–78–C–0192
Report No. 7
For period 1 January 1980 through 30 September 1980

Approved for public release; distribution unlimited.

Sponsored by
DEFENSE ADVANCED RESEARCH PROJECTS AGENCY
Arlington, Virginia 22209

Monitored by
NAVAL RESEARCH LABORATORY
Washington, D.C. 20375

UNCLASSIFIED

SECURITY CLASSIFICATION OF THIS PAGE (When Data Entered)

REPORT DOCUMENTATION PAGE	READ INSTRUCTIONS BEFORE COMPLETING FORM
1. REPORT NUMBER	2. GOVT ACCESSION NO. AD-A092 690 / 3. RECIPIENT'S CATALOG NUMBER
4. TITLE (and Subtitle) OPTICAL MICROWAVE INTERACTIONS IN SEMICONDUCTOR DEVICES,	5. TYPE OF REPORT & PERIOD COVERED Report, No. 7 1 Jan 1980 – 30 Sep 1980 6. PERFORMING ORG. REPORT NUMBER
7. AUTHOR(s) L. Figueroa, C.W. Slayman, H.W. Yen	8. CONTRACT OR GRANT NUMBER(s) N00173-78-C-0192
9. PERFORMING ORGANIZATION NAME AND ADDRESS Hughes Research Laboratories 3011 Malibu Canyon Road Malibu, California 90265	10. PROGRAM ELEMENT, PROJECT, TASK AREA & WORK UNIT NUMBERS
11. CONTROLLING OFFICE NAME AND ADDRESS Defense Advanced Research Projects Agency Arlington, Virginia 22209	12. REPORT DATE November 1980 13. NUMBER OF PAGES 95
14. MONITORING AGENCY NAME & ADDRESS (if different from Controlling Office) Naval Research Laboratory Washington, D.C. 20375	15. SECURITY CLASS. (of this report) UNCLASSIFIED 15a. DECLASSIFICATION DOWNGRADING SCHEDULE

16. DISTRIBUTION STATEMENT (of this Report)

Approved for public release; distribution unlimited.

17. DISTRIBUTION STATEMENT (of the abstract entered in Block 20, if different from Report)

18. SUPPLEMENTARY NOTES

19. KEY WORDS (Continue on reverse side if necessary and identify by block number)

AR coating, detector analog response, detector pulse response, electron traps, external optical cavity, high frequency analog modulation, laser equivalent circuit, mode-locking, p-n junction detector, saturable absorbing defects, self-pulsations, and time multiplexing.

20. ABSTRACT (Continue on reverse side if necessary and identify by block number)

The results of an extensive characterization of high-speed analog modulation of (GaAl)As injection lasers, high speed optical detectors, and mode-locking of (GaAl)As injection lasers are presented. Commercial (GaAl)As injection lasers have been successfully modulated up to 5 GHz. The 5 GHz value represents a practical upper limit to the modulation bandwidth of existing commercial lasers. We also

DD FORM 1 JAN 73 1473 EDITION OF 1 NOV 65 IS OBSOLETE

UNCLASSIFIED

SECURITY CLASSIFICATION OF THIS PAGE (When Data Entered)

characterized the laser equivalent circuit and found that the parasitics play a significant role in the high-speed modulation of the injection laser.

High-speed optical detectors were characterized, and we found that some commercial p-n junction detectors can respond to analog modulated optical signals at frequencies beyond 7 GHz. We characterized the optical response of GaAs MESFETs and found that they can respond to analog modulated optical signals at frequencies beyond 4 GHz with a sensitivity comparable to the best p-n junction detectors. Photoconductivity is the mechanism responsible for the optical response. We compared our experimental results with predictions from a simple theory and found them to agree in many instances. We believe that a photoconductive detector with an optimized geometry can be used in microwave-optical analog signal processing systems.

A theoretical and experimental study of mode locking in (GaAl)As injection lasers was performed. Our results indicate that the mode locking of (GaAl)As injection lasers is related to either saturable absorbing or electron trap defects within the active region of the laser. These defects are also responsible for self-pulsations in injection lasers. "Good" mode locking is achieved only in lasers having a high density of these defects. We achieved detector-limited mode-locked pulses (less than 200 psec full width at half maximum) with repetition rates of ∿1 GHz and 100% modulation depth. We were also able to time multiplex the mode-locked pulses to double the pulse repetition rate.

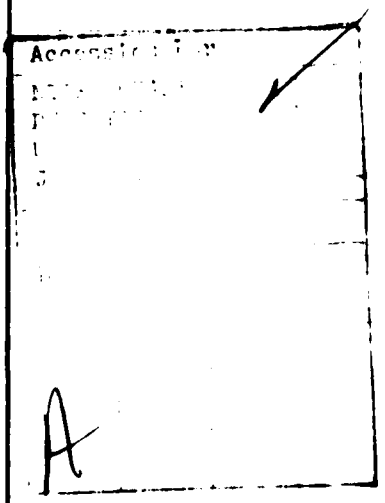

TABLE OF CONTENTS

LIST OF ILLUSTRATIONS

PREFACE

The following personnel contributed to the research reported here: L. Figueroa, C.W. Slayman, H.W. Yen, C. Krumm, R.K. Jain, D. Pierson, and D.F. Lewis.

SECTION 1

INTRODUCTION AND SUMMARY

In this program, one of our primary goals is the use of microwave modulated optical signals to control microwave semiconductor devices to achieve various functions such as injection locking and switching of oscillators, mixing and detection of microwave modulated optical signals. A second goal is the combination of microwave and optical devices for use in microwave signal processing systems. To perform such functions, we must develop methods and devices that can provide modulation and detection of optical beams at microwave frequencies.

Our approach for modulating the optical beam has been to study the modulation capability of (GaAl)As injection lasers. The simplest technique envisioned involved the direct modulation of the laser current. Section 2 describes our extensive theoretical and experimental study of modulation of various commercial (GaAl)As injection lasers. An understanding of the capabilities and limitations of existing laser structures is an essential prerequisite to progress toward improving their performance. Our results indicate that efficient direct current modulation of commercial (GaAl)As injection lasers is limited by the relaxation oscillation frequency of the laser. This frequency sets a practical upper bandwidth limit of $\sim$5 GHz.

Mode locking is a second technique we have used to modulate the light output. This technique pulse modulates the light output and can produce an output with large peak powers and very rich harmonic content, which should make it directly applicable to the phase locking of microwave semiconductor devices. Our initial work on mode-locking began in January 1979; we have been able to generate detector-limited pulses at frequencies ranging from 1.0 to 3 GHz. Section 4 describes a comprehensive theoretical and experimental study of mode-locking in (GaAl)As injection lasers. We found, as originally speculated, that mode-locking in various commercial (GaAl)As injection lasers is strongly

influenced by the type of laser structure used. In particular, we found that lasers having a high density of saturable absorbing defects are most susceptible to mode-locking. One of our key findings is the direct correlation between the phenomenon of self-pulsation and "good" mode-locking. The above results imply that mode-locking in (GaAl)As injection lasers is very similar to mode-locking in dye lasers. Our most recent results have produced pulses with 200 psec pulse width (detector limited) operating at frequencies beyond 1 GHz. The ultimate goal of this study is to fabricate and deliver a working mode-locked laser unit with a minimum pulse width of 100 psec operating at 2-GHz repetition rates. The higher repetition rate will be obtained by using an optical time multiplexer that will double the frequency. Section 4.E describes our most recent work on mode-locking and multiplexing.

Of primary concern to this program and to future microwave signal processing systems, such as optical fiber delay lines, is a high-speed optical detector. Section 3 describes our work on high-speed optical detectors. A large percentage of this work was not funded under the present DARPA program. However, for completeness and because of the importance of the work, we describe our most significant results.

Section 3.A discusses the results obtained from characterizing important commercial high-speed detectors. This characterization is an important step in redesigning detectors for improved high-frequency performance. Section 3.B discusses our work on a theoretical and experimental description of the high-frequency optical characteristics of GaAs MESFETs. This work was begun after we had obtained encouraging results during our study of GaAs/(GaAl)As waveguide MESFET detectors (work we reported on in the February 1980 DARPA quarterly). The results obtained using HAC MESFETs provided the first extensive characterization of the GaAs MESFET as an optical detector. We have characterized both the pulse and analog responses of the devices and we have observed flat analog bandwidths for frequencies up to and probably beyond 4 GHz. The pulse response shows that it is possible to detect pulses with an 80-psec half-width. We believe that it is now possible to design high-speed optical detectors using an optimized FET geometry.

SECTION 2

ANALOG MODULATION OF (GaAl)As INJECTION LASERS

This section describes the important parameters affecting the direct-current modulation of (GaAl)As injection lasers at GHz rates. Extensive experimental results on the high-frequency characteristics of commercial (GaAl)As injection lasers is presented.

A. DIRECT-CURRENT MODULATION OF (GaAl)As INJECTION LASERS AT GHz RATES

The easiest way to modulate an injection laser is to modulate the laser current directly. The frequency response of the laser can be analyzed using a pair of simple rate equations for a single longitudinal mode:[1]

$$\frac{dn}{dt} = \frac{J}{ed} - Gns - \frac{n}{\tau_s} \tag{1a}$$

$$\frac{ds}{dt} = Gns - \frac{S}{\tau_p} + \frac{\beta n}{\tau_s} \quad , \tag{1b}$$

where n is the electron inversion density, s is the photon density, J is the laser driving current, e is the electronic charge, d is the thickness of the laser active region, G is a constant related to the stimulated emission process, τ_s is the spontaneous lifetime of the electrons, τ_p is the photon lifetime in the laser cavity, and β is the spontaneous emission factor. This last factor gives us the percentage of the total spontaneous emission that goes into the lasing mode. The above equations neglect transverse optical confinement, current spreading, lateral out-diffusions of injected carriers and the effects of circuit parasitics. Since this set of equations is nonlinear, exact analytical solutions are difficult to obtain. However, approximations

can be used to calculate the small-signal response of the laser. We first simplify the equations by using an appropriate normalization procedure; we define:

$$t \equiv \frac{t}{\tau_s}$$

$$n_e \equiv G\tau_p n$$

$$s_p \equiv G\tau_s S$$

$$j \equiv G\tau_s\tau_p \left(\frac{J}{ed}\right)$$

$$C \equiv \frac{\tau_s}{\tau_p} \quad .$$

Using these definitions, Eq. 1 can be rewritten as

$$\frac{dn_e}{dt} = j - S_p n_e - n_e$$

$$\frac{ds_p}{dt} = C\,[s_p\,(n_e - 1) + \beta n_e] \quad . \tag{2}$$

To calculate the small-signal response, we use a perturbation technique. The relevant quantities are:

$$j = j^{(0)} + j^{(1)}$$

$$n_e = n_e^{(0)} + n_e^{(1)} + n_e^{(2)} \tag{3}$$

$$s_p = s_p^{(0)} + s_p^{(1)} + s_p^{(2)} \quad .$$

The steady state solutions, $n_e^{(0)}$ and $s_p^{(0)}$, are due to the dc current $j^{(0)}$. If we define a normalized modulation depth $F(\omega)$ as $s_p^{(1)}(\omega)/j^{(1)}(\omega)$, then $F(\omega)$ can be shown to be

$$F(\omega) = \frac{C\,(s_p^{(0)} + \beta)}{(i\omega\tau_s + s_p^{(0)} + 1)\left[i\omega\tau_s - C(n_e^{(0)} - 1) + C(s_p^{(0)} + \beta)\,(n_e^{(0)})\right]} \quad . \tag{4}$$

For the simplest case, we assume $\beta = 0$ and Eq. 4 reduces to

$$F(\omega) = \frac{Cs_p^{(0)}}{(Cs_p^{(0)} - \omega\tau_s^2) + i\omega\tau_s(s_p^{(0)} + 1)} \quad . \tag{5}$$

We can define a frequency ω_0 where $F(\omega)$ has a resonance:

$$\omega_0 = \left(\frac{1}{\tau_p\tau_s}\right)^{1/2} (S_p^{(0)})^{1/2} \quad . \tag{6}$$

Since $S_p^{(0)}$ is the normalized dc photon value, we can write

$$S_p^{(0)} = (j_o - 1) \quad . \tag{7}$$

Thus, Eq. 6 reduces to

$$\omega_o = \left(\frac{1}{\tau_s\tau_p}\right)^{1/2} (j_0 - 1)^{1/2} \quad . \tag{8}$$

Eqs. 7 and 8 are based on the fact that the normalized threshold current density J_{th} is equal to 1 in the case considered.

Figure 1 is a plot of the calculated magnitude of $F(\omega)$ for various values of I/I_{th} (I/I_{th} is equivalent to j_0) and assuming $\beta = 0$. Figure 2 shows the effect of a finite β. Note that increasing β reduces the amplitude of the resonance response. This result is expected since β is a measure of the amount of damping in the system. Furthermore, β is inversely proportional to the laser volume since we have a higher spontaneous emission rate for a small active region volume, in a manner similar to the increased stimulated emission rate. Thus, one conclusion is that injection lasers with a small active region volume should have a flatter modulation response.

B. CIRCUIT CONSIDERATIONS

In the previous subsection, we discussed the modulation response of the injection laser. However, the simple rate equations do not include the effects of circuit parasitics. Figure 3 is a schematic for an idealized equivalent circuit that represents the diode laser and package. C_p is the package shunt capacitance; L_s is the series inductance of the bond wire; and R_j and C_j are the forward-biased junction resistance and capacitance, respectively. It is the forward current flowing through R_j that causes lasing. Current flowing through C_p and C_j will not give rise to photon generation.

Figures 4 and 5 are plots of laser impedance from 100 MHz to 10 GHz in 100-MHz steps for Hitachi buried-heterostructure (BH) and channeled-substrate-planar (CSP) lasers. Table 1 lists the values obtained for the circuit parameters shown in Figure 3. These values were obtained using a circuit analysis computer program to calculate the values by using a least-squares fit to the data of Figures 4 and 5. The values obtained in Table 1 fit the data of Figures 4 and 5 with an accuracy of 10% for frequencies between 100 MHz and 6 GHz. The reflection coefficient of the laser is

$$\Gamma = \frac{Z_L - Z_0}{Z_L + Z_0} \quad , \tag{9}$$

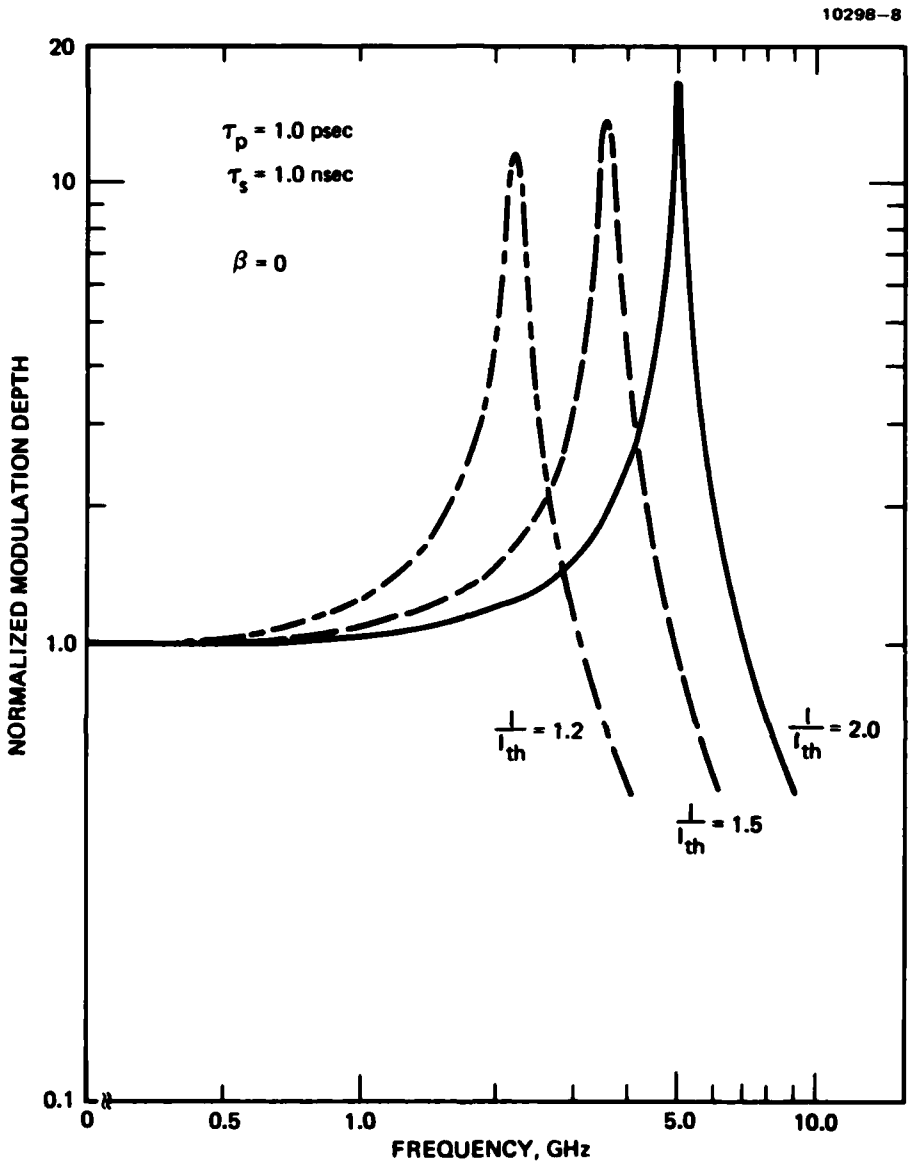

Figure 1. Frequency dependence of the normalized modulation depth of an injection laser. The spontaneous emission factor, β, is equal to zero.

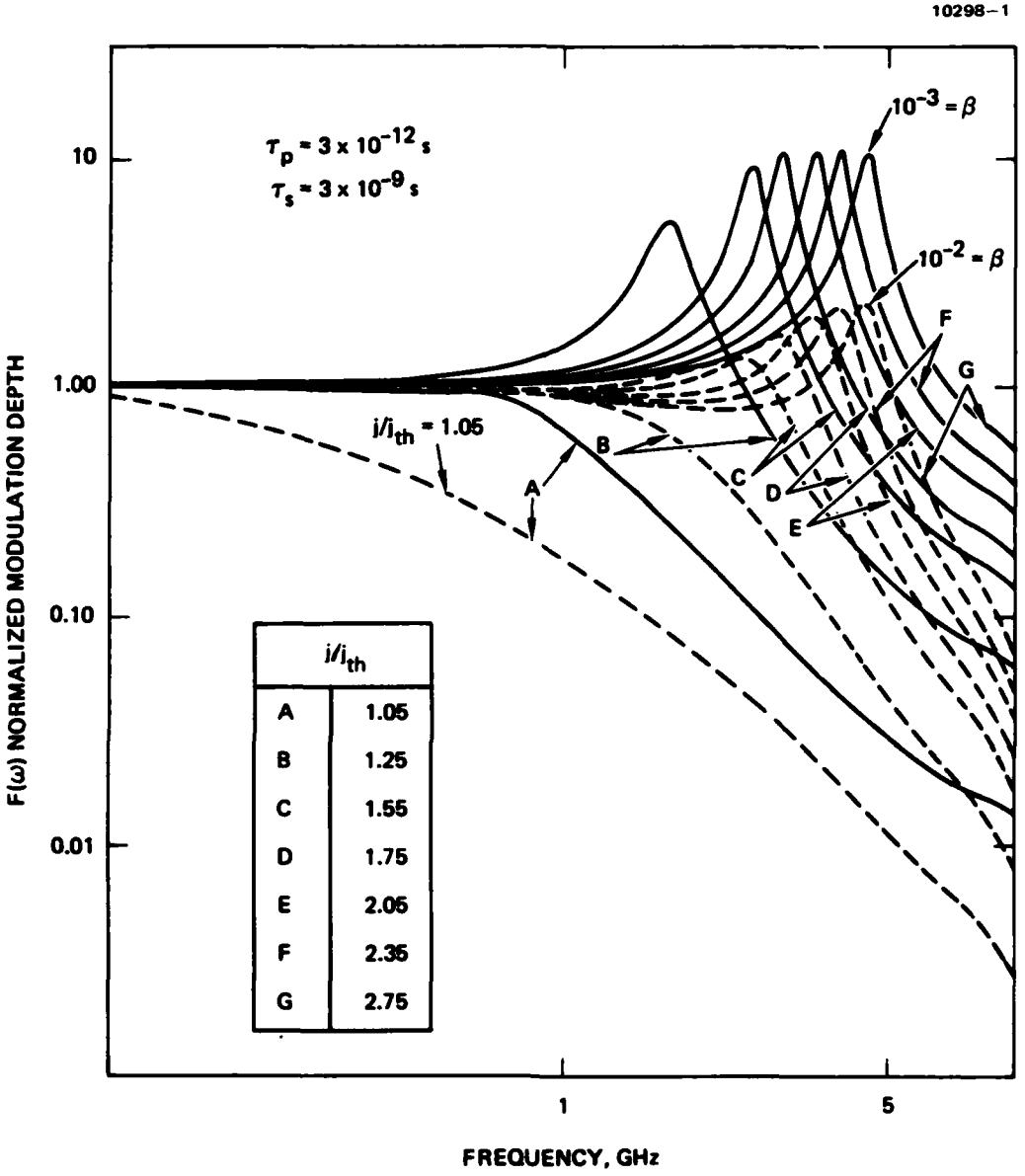

Figure 2. Frequency dependence of the normalized modulation depth of an injection laser where the spontaneous factor, β, is not zero.

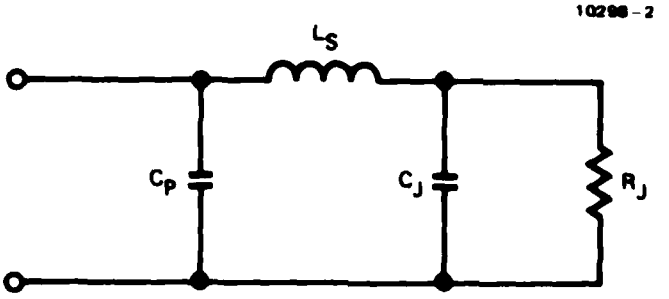

Figure 3. *Equivalent* circuit of the (GaAl)As injection laser.

9646-21

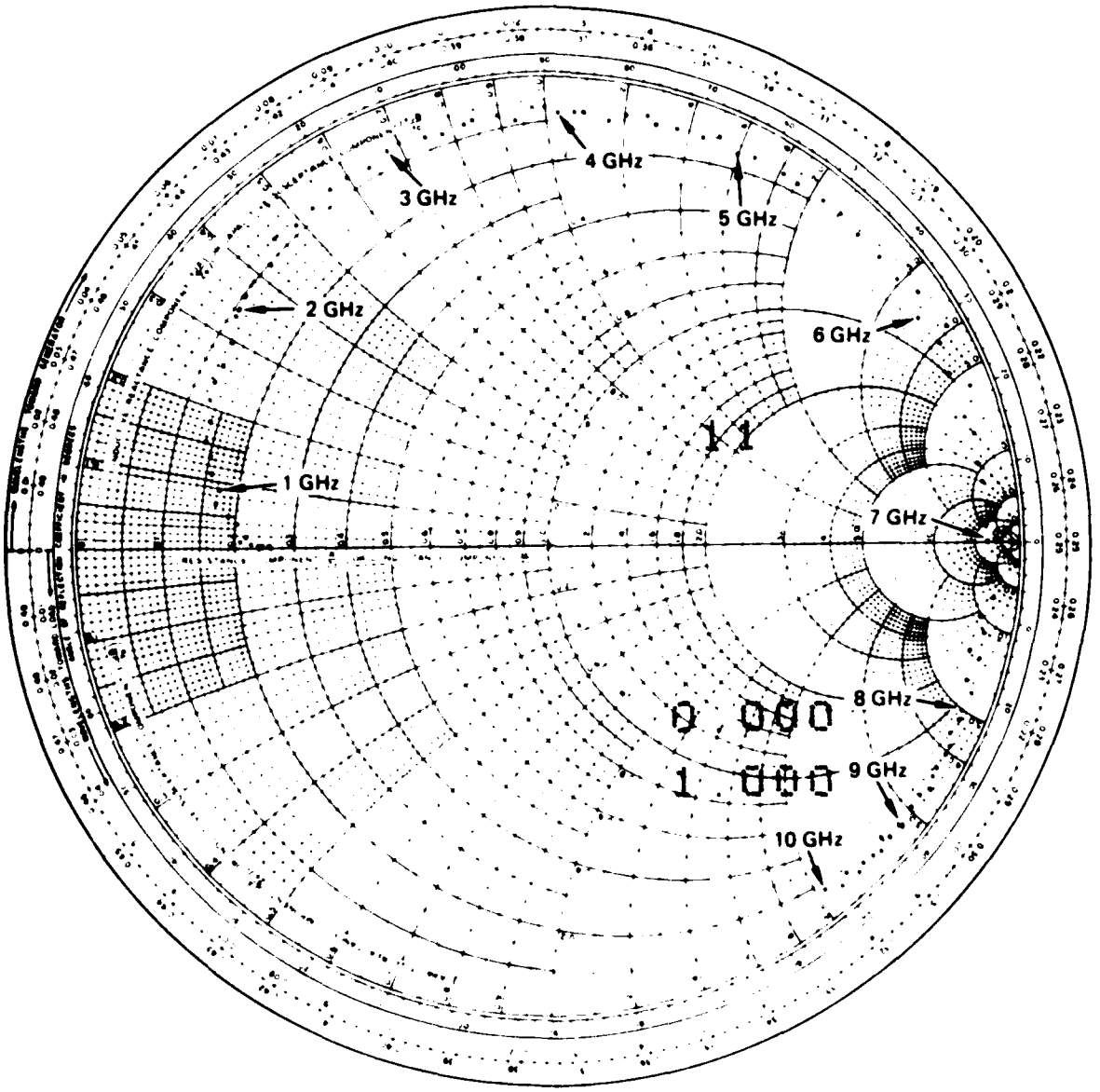

Figure 4. Hitachi BH laser (HLP 2400U) impedance from 100 MHz to 10 GHz in 100-MHz steps. Smith chart is normalized to 50 Ω.

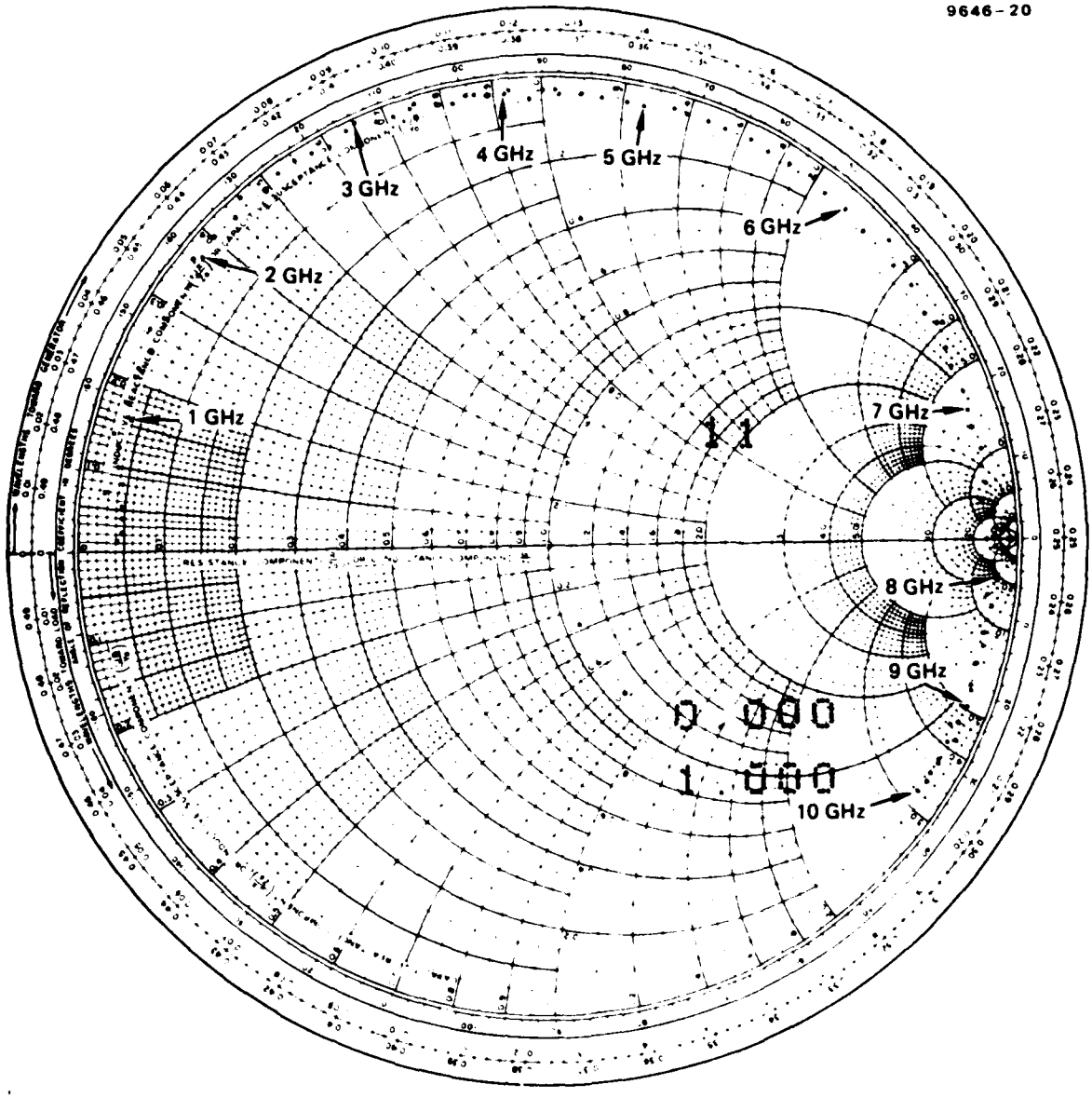

Figure 5. Hitachi CSP laser (HLP 1400) impedance from 100 MHz to 10 GHz in 100-MHz steps. Smith chart is normalized to 50 Ω.

Table 1. Equivalent Circuit Parameters

Laser Type	C_p, F	L_p, H	C_j, F	R_j, Ω
CSP	0.348×10^{-12}	1.5×10^{-9}	10×10^{-12}	10
BH	0.315×10^{-12}	1.318×10^{-9}	40×10^{-12}	2

where Z_L is the laser impedance, and Z_0 is the characteristic impedance of the system (typically $Z_0 \approx 50\ \Omega$). The magnitude of the current flowing through the laser package is

$$i = i_0 \left| 1 - \Gamma \right| \ , \tag{10}$$

where i_0 is the magnitude of current from the rf source into a matched load. Figure 6 shows $1 - \Gamma$ as a function of frequency for the BH and CSP lasers. Note that not all the current flowing into the package will flow through the junction. Therefore, Eq. 10 represents the maximum possible current going into photon generation.

To maintain a flat frequency response, a matching circuit can be used to compensate for the frequency dependence of Γ. The conventional technique is to reduce Γ to zero (i.e., power match). However, laser response is a function of the current going through (and not of the power delivered to) the diode. If the laser appeared as a short circuit across the frequency band of interest, twice as much current would flow compared to the case of a matched load. Thus, the optical output of the laser would be 3-dB greater in the short-circuit case. However, this 3-dB increase would be at the cost of an infinite VSWR. In our experiments, no matching techniques were used. The error produced by reflections was quite small since the reflection coefficient is relatively independent of frequency at frequencies below 5 to 6 GHz.

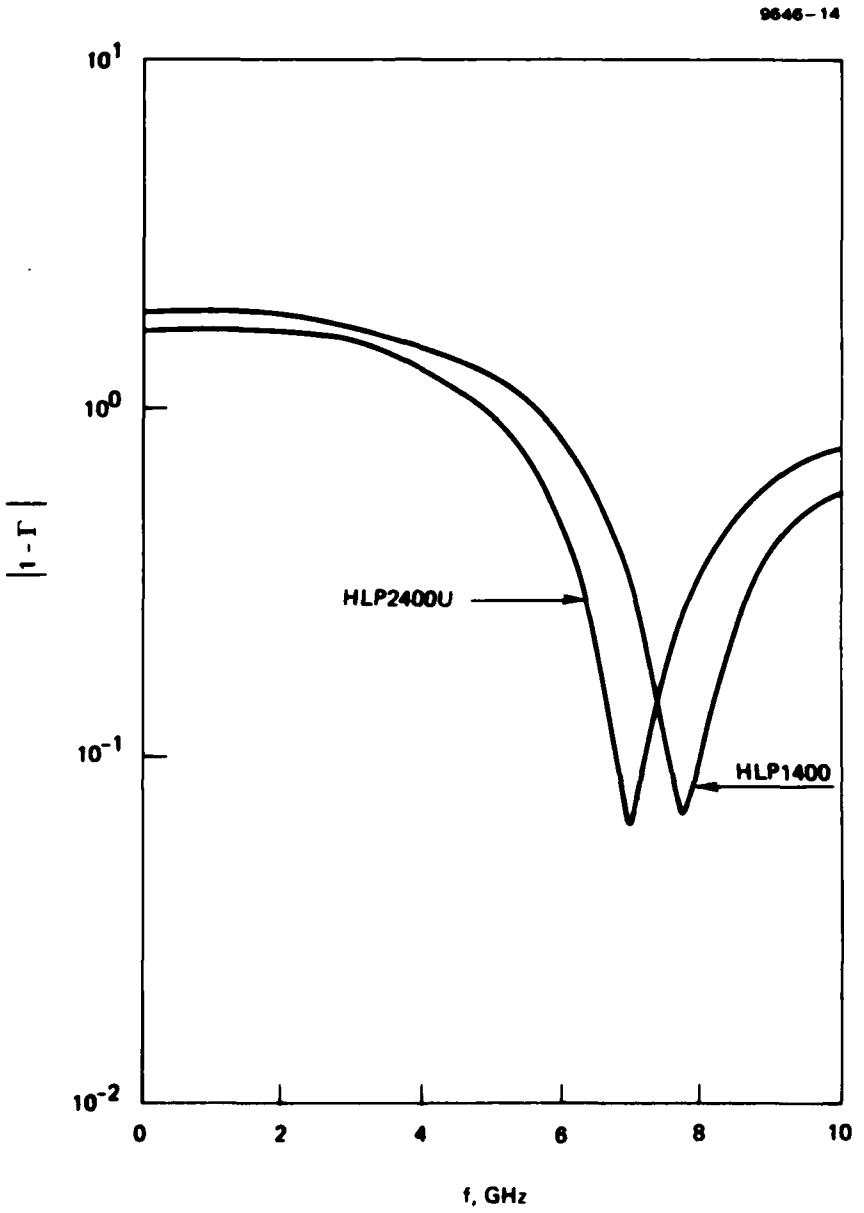

Figure 6. $|1 - \Gamma|$ as a function of frequency.

C. EXPERIMENTAL RESULTS

Several GaAs/GaAlAs lasers were characterized to determine their suitability using direct current modulation. Because $1 - \Gamma$ was found to be relatively flat for the BH and CSP lasers, no attempt was made to match to the laser impedance. Each laser was mounted at the end of a microstrip fabricated from Au-plated alumina. The rf power was coupled via an APC-7 microstrip launcher. The optical signal was demodulated by a Rockwell GaAs/GaAlAs heterostructure photodiode. A Hewlett Packard network analyzer system HP-8410 (harmonic converter/S-parameter test set/phase magnitude display, and rf sweep generator) was used to characterize the frequency response of the laser-photodiode pair. Figure 7 is a block diagram of the frequency response experiment. Figure 8 shows the optics used to couple the laser radiation to the photodiode. A variable neutral density (ND) filter (or optical attenuator) was used to prevent excess optical power from damaging the photodiode.

Figures 9 through 13 show the throughput or insertion loss L(f) as a function of frequency for the Hitachi BH, CSP, BH/LOC (BH/large optical cavity), the Mitsubishi TJS (transverse junction stripe), and General Optronics proton-bombarded stripe laser. The absolute value of L for each laser/photodiode combination is relative because different values of attenuation were used. The dc insertion loss was measured by plotting the change in detector current as a function of laser current.

The relaxation oscillation resonance can be seen in all of the lasers shown in Figures 9 through 13. The strong resonance in the General Optronics laser is probably due to the onset of self-pulsations, which could have resulted from the excessive drive level used. The laser structures studied differed vastly in resonance behavior. This behavior can be qualitatively explained by considering the spontaneous emission factor of the laser and using Figure 2. For example, the CSP and the General Optronics lasers have a relatively wide stripe width (i.e., the width over which the current flows). Typical stripe widths are 6 to 15 μm, which leads to a $\beta \gtrsim 10^{-3}$. On the other hand, the BH and TJS lasers have relatively narrow stripe widths ($\sim$1 μm) and thus

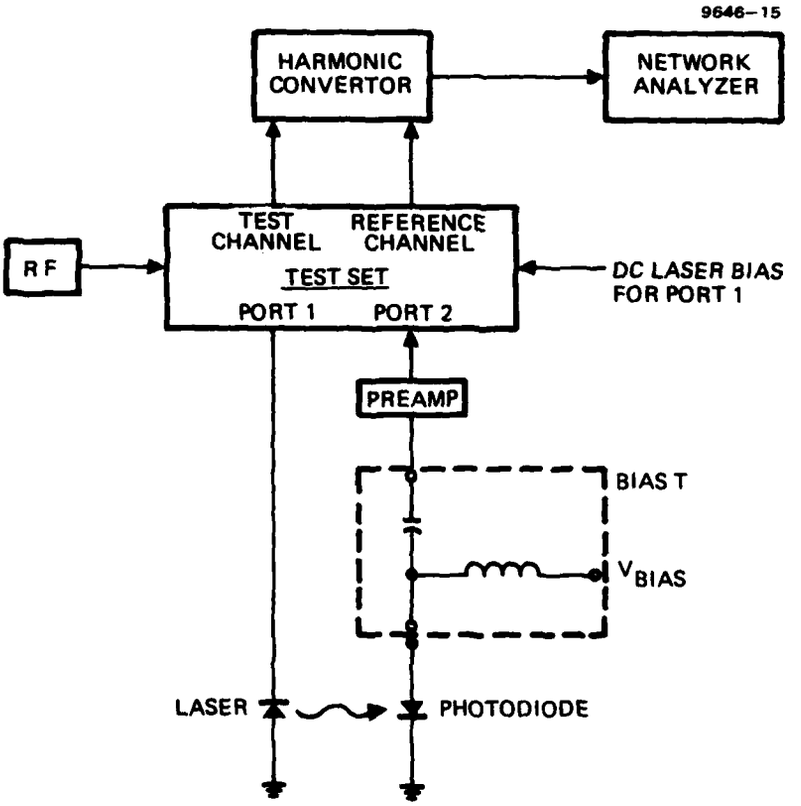

Figure 7. Block diagram of the frequency response measurement.

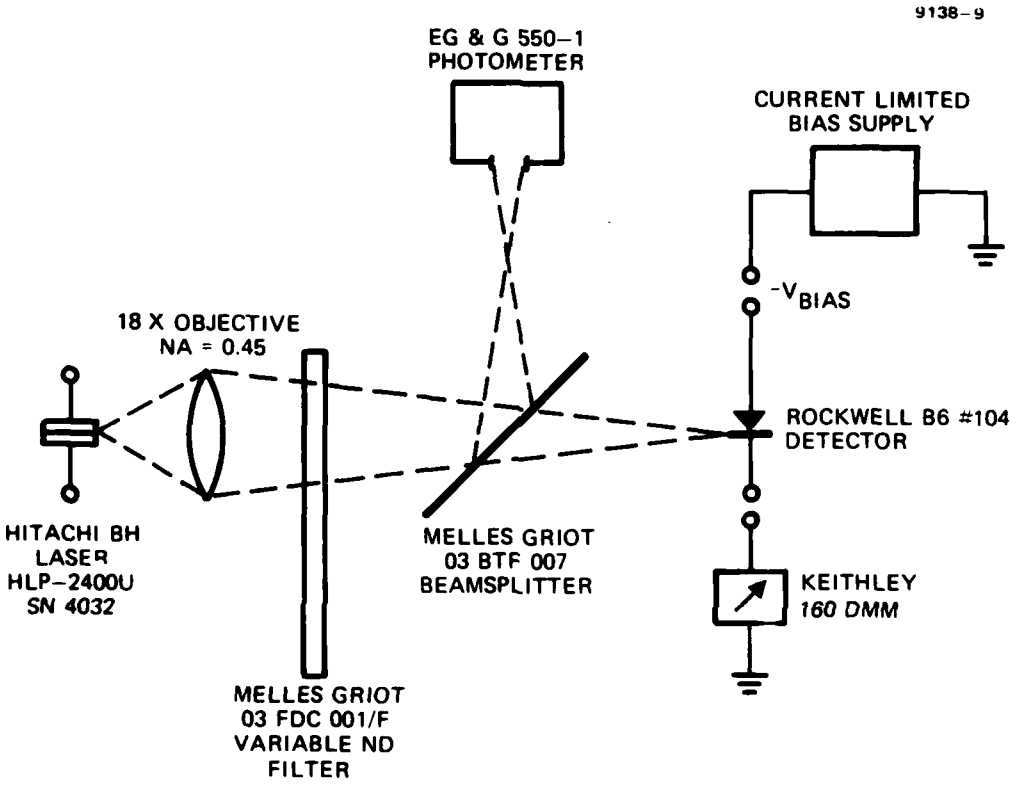

Figure 8. Laser-photodiode optical arrangement.

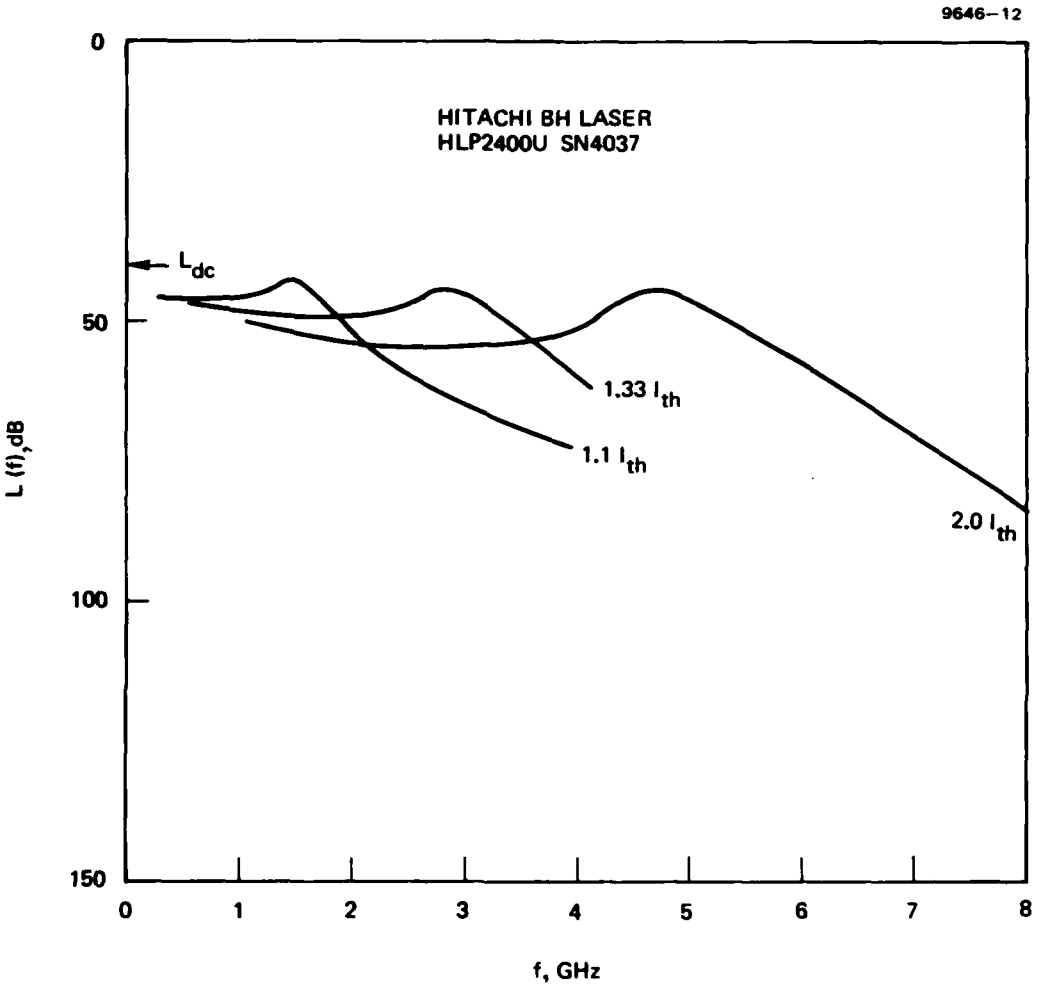

Figure 9. Response of the Hitachi BH laser.

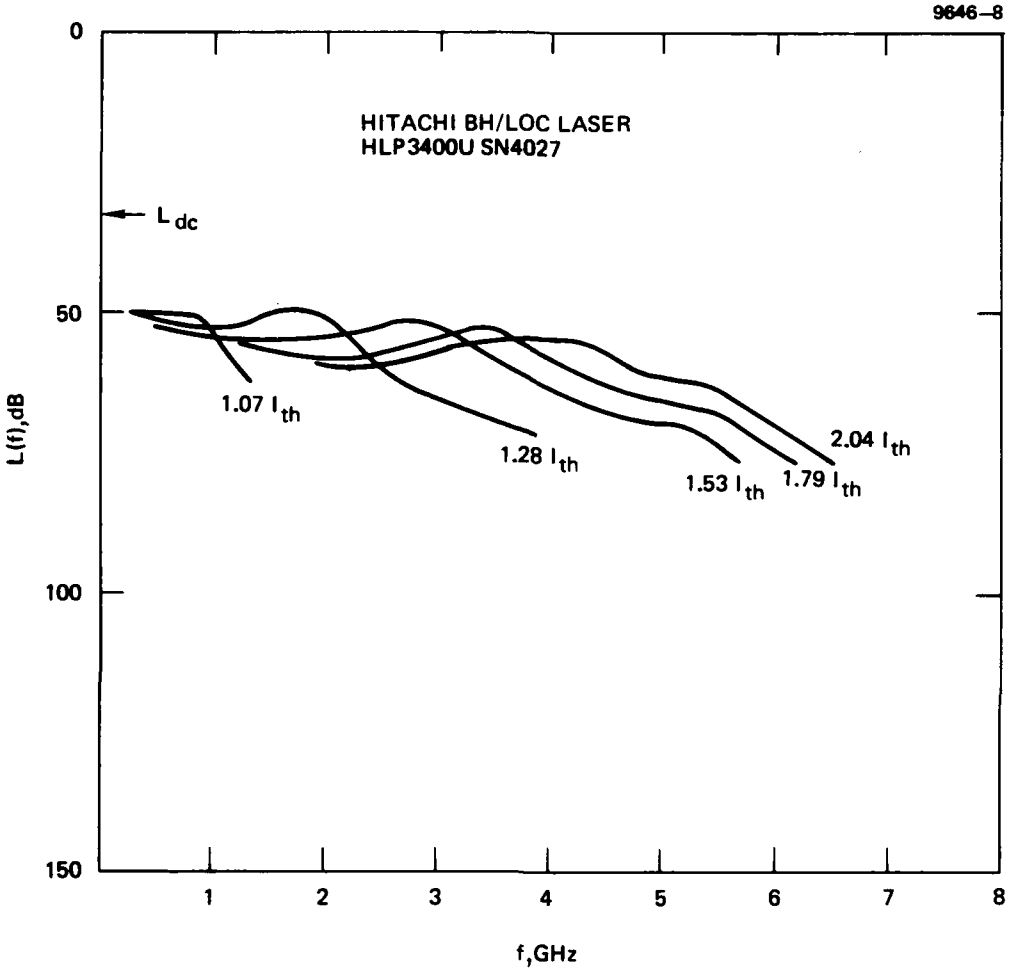

Figure 10. Response of the Hitachi BH/LOC laser.

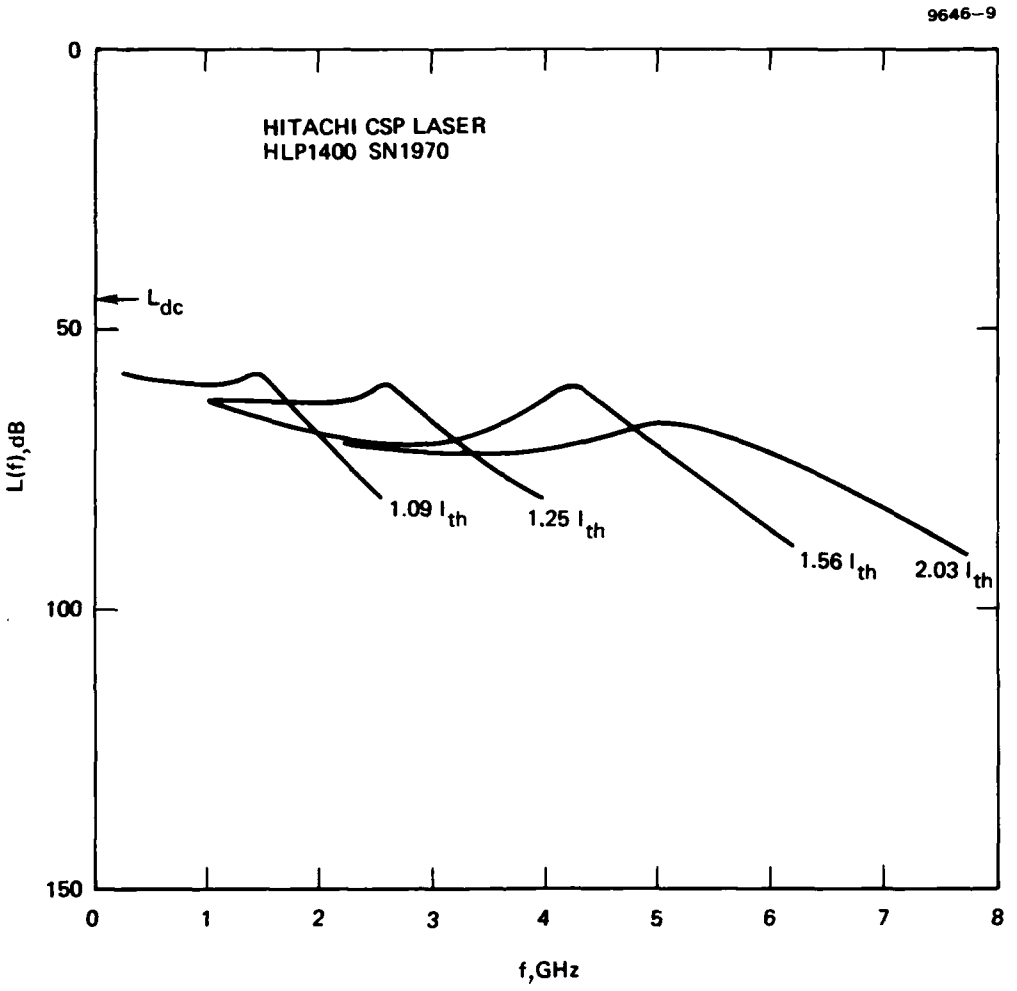

Figure 11. Response of the Hitachi CSP laser.

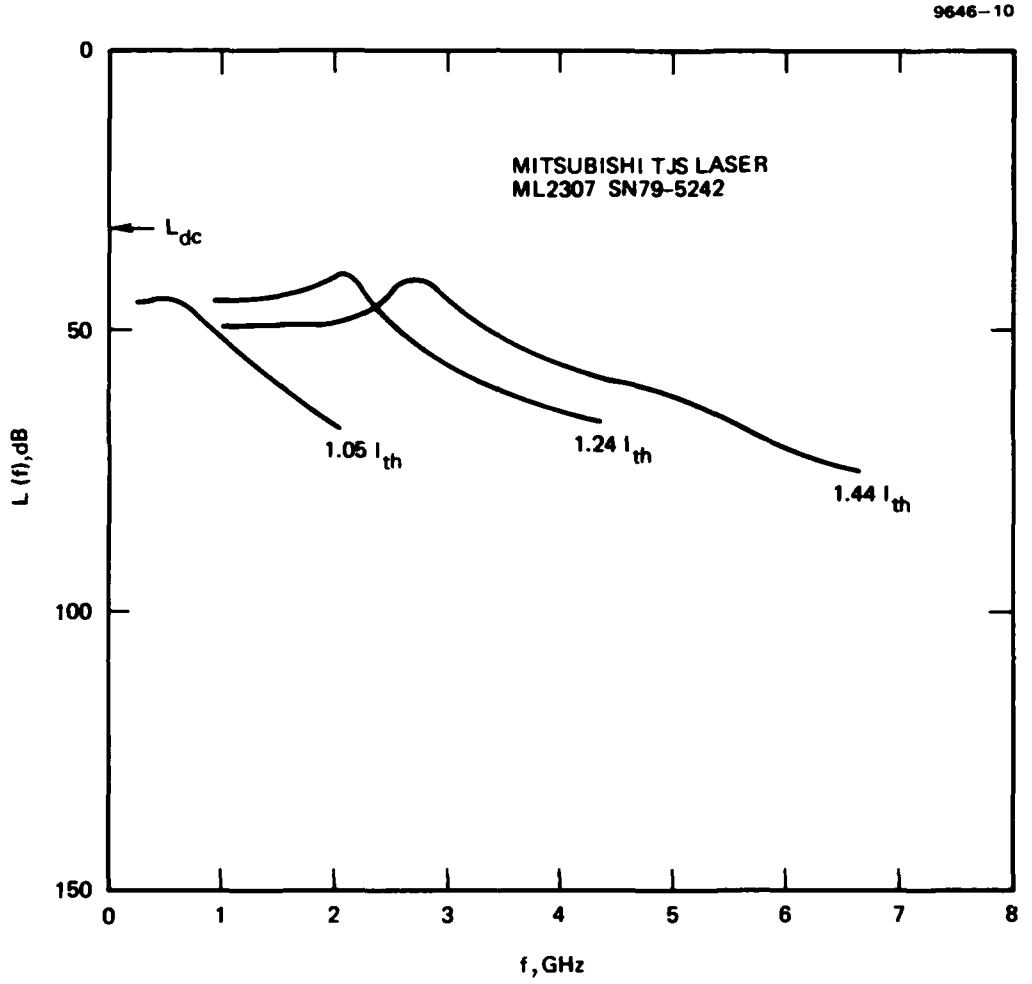

Figure 12. Response of the Mitsubishi TJS laser.

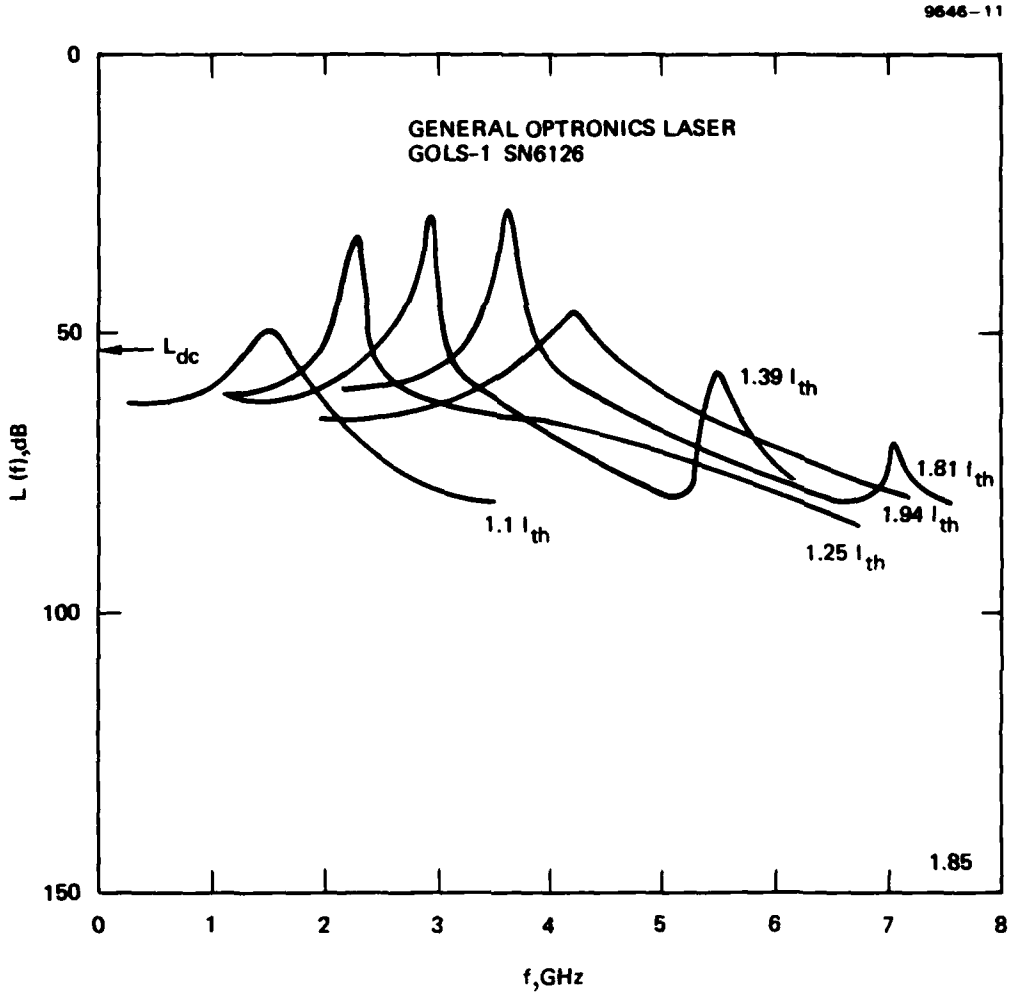

Figure 13. Response of the General Optronics laser.

have a $\beta \gtrsim 10^{-2}$. Therefore, we expect the CSP and the General Optronics lasers to have a more pronounced resonance behavior than the BH and TJS lasers. A comparison of Figures 9 through 13 confirms our speculation. Figures 14 through 18 are plots of the relaxation oscillation frequency ($f_o = \omega_o/2\pi$) as a function of laser drive (I/I_{th}) for the five lasers tested. As expected, f_o follows the behavior of Eq. 8 with $1/[2\pi(\tau_p\tau_s)^{1/2}]$ ranging from 3.7 GHz for the BH/LOC laser to 5.35 GHz for the CSP laser. In some of the lasers, the magnitude of the resonance decreases with increasing drive current. We believe this effect is due to the circuit parasitics. Furthermore, all the lasers tested showed a dip in the modulation response at a frequency lower than the resonance frequency. We believe that this effect is due to the out-diffusion of injected carriers. Our results indicate that efficient analog modulation of existing commercial (GaAl)As injection lasers is limited to $\sim$5 GHz. Frequencies beyond 5 GHz will require excessive drive currents ($I > 2I_{th}$), leading to a relatively large output power density. Operating injection lasers at high power densities could reduce their reliability and significantly shorten their life.

The results obtained in this section provide some guidelines and techniques that can be used to improve the high-frequency modulation characteristics of (GaAl)As injection lasers. First, a reduction of the laser cavity length will decrease the photon lifetime τ_p of the laser and thus increase the maximum frequency f_o. For example, a reduction of the laser cavity length from a typical 300 μm to 75 μm can increase f_o to beyond 10 GHz. Second, the effect of circuit parasitics has been examined in detail for the first time. It is of utmost importance to design new laser structures and microstrip circuits that can minimize circuit parasitics. The laser structures and microstrip circuits can be characterized using existing microwave test equipment.

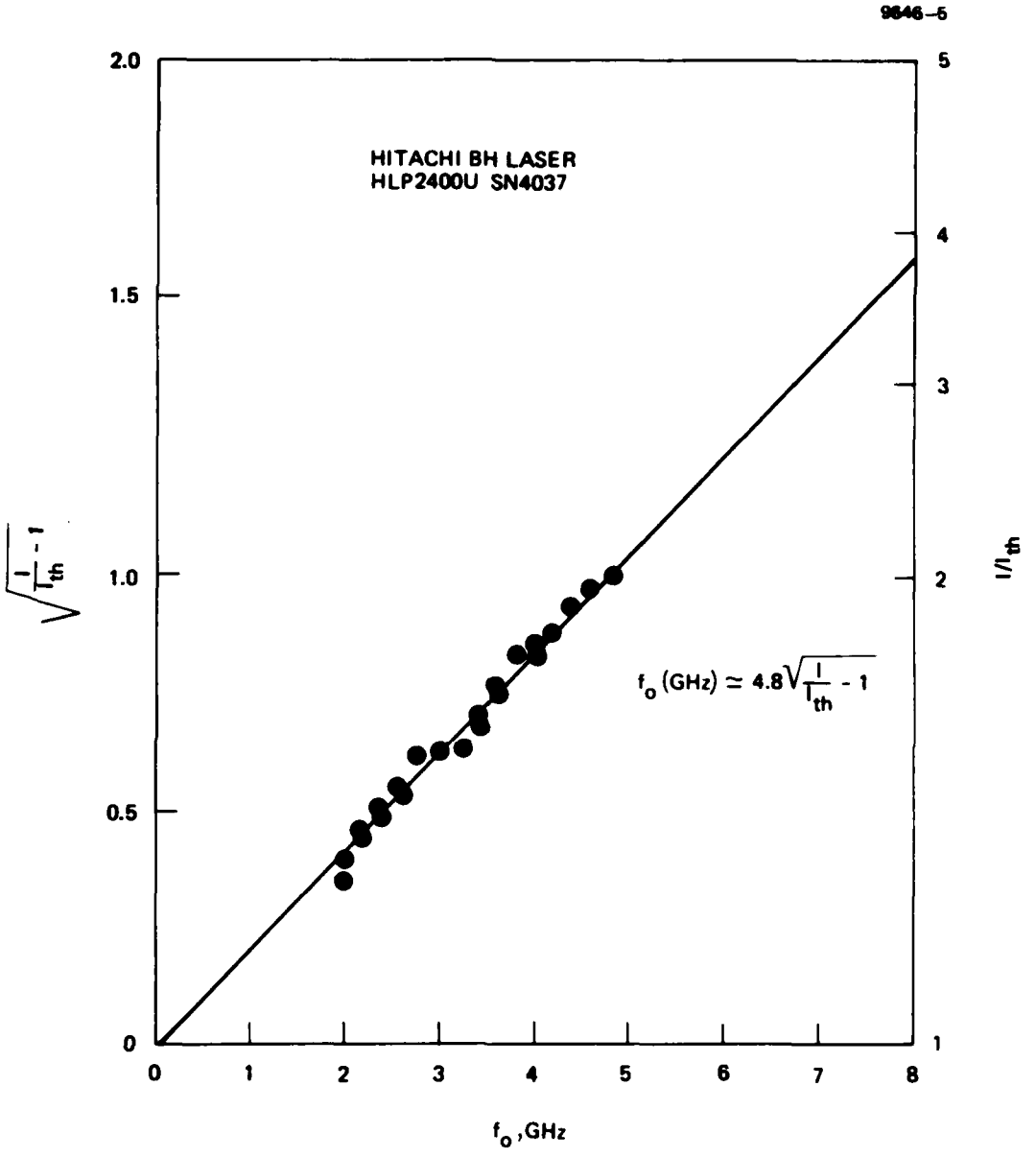

Figure 14. Relaxation oscillation frequency as a function of bias for the Hitachi BH laser.

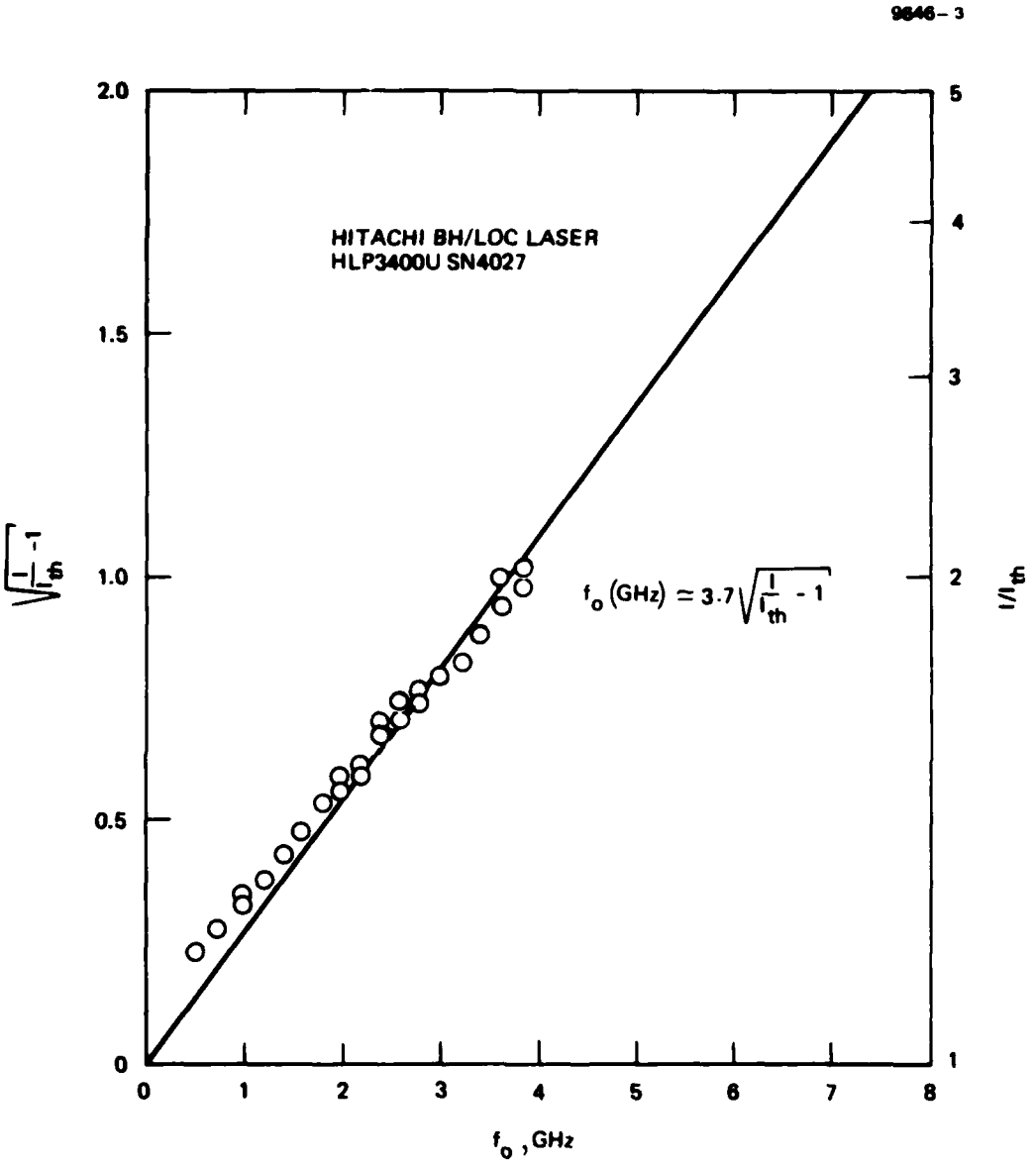

Figure 15. Relaxation oscillation frequency as a function of bias for the Hitachi BH/LOC laser.

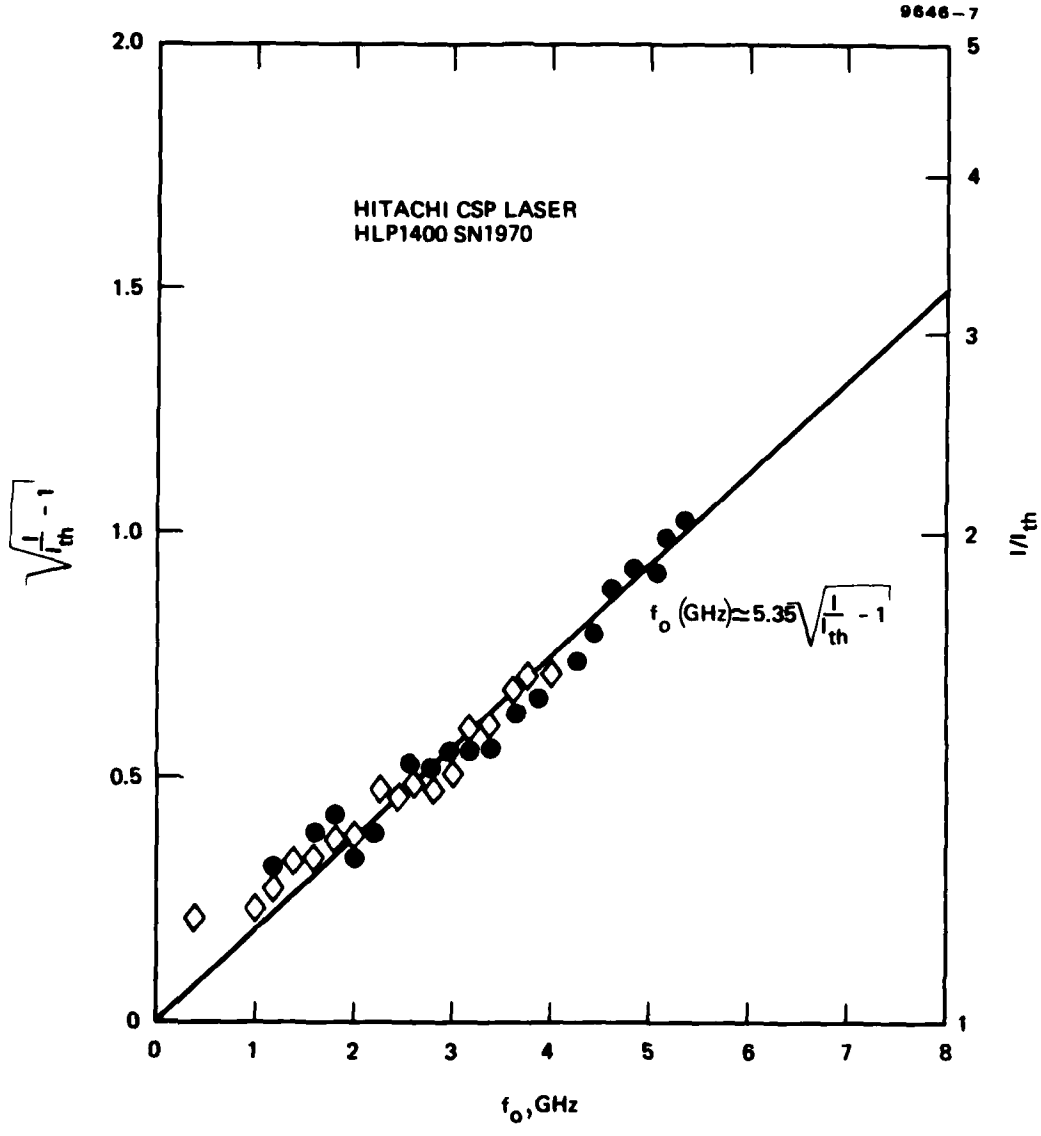

Figure 16. Relaxation oscillation frequency as a function of bias for the Hitachi CSP laser.

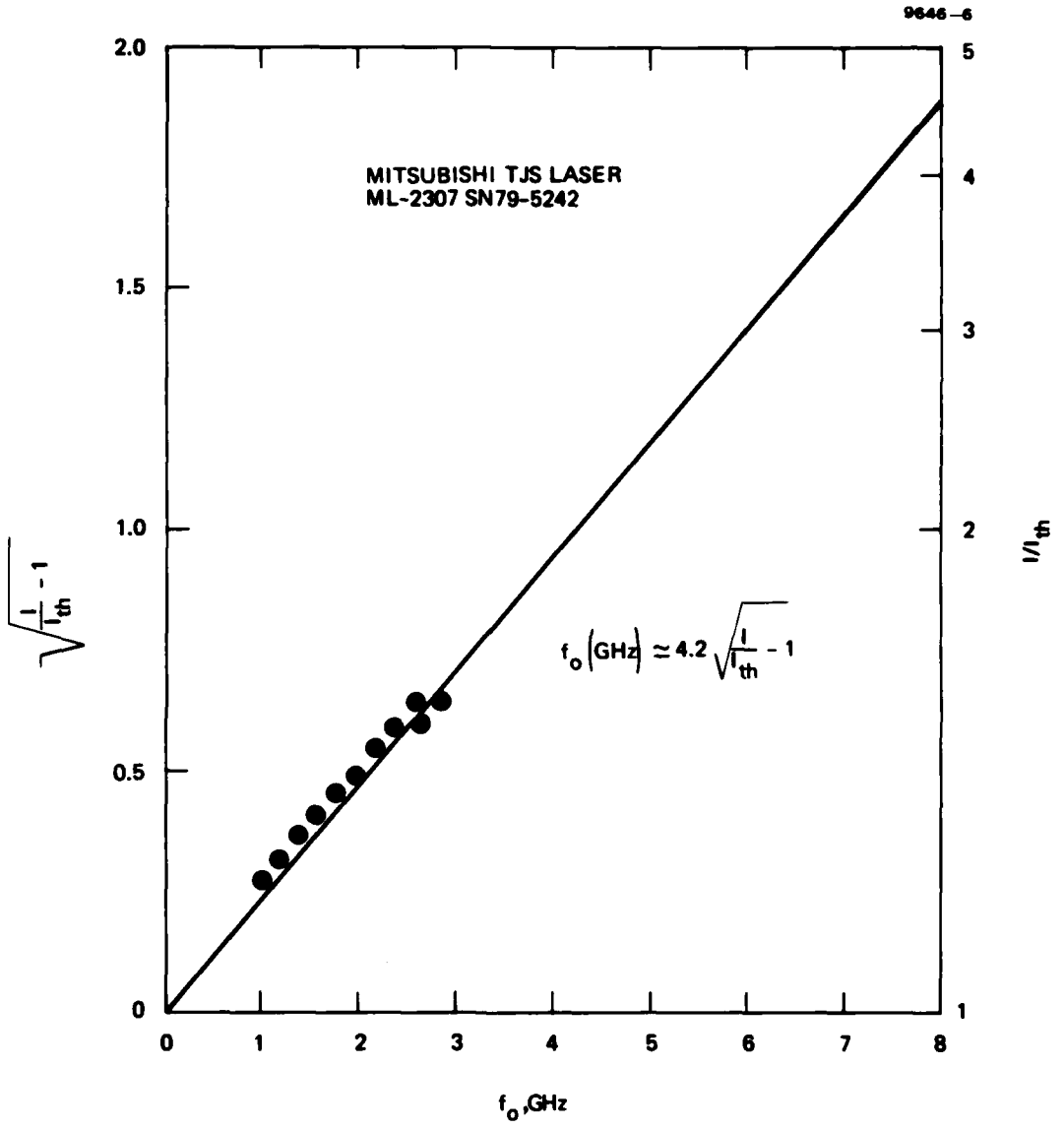

Figure 17. Relaxation oscillation frequency as a function of bias for the Mitsubishi TJS laser.

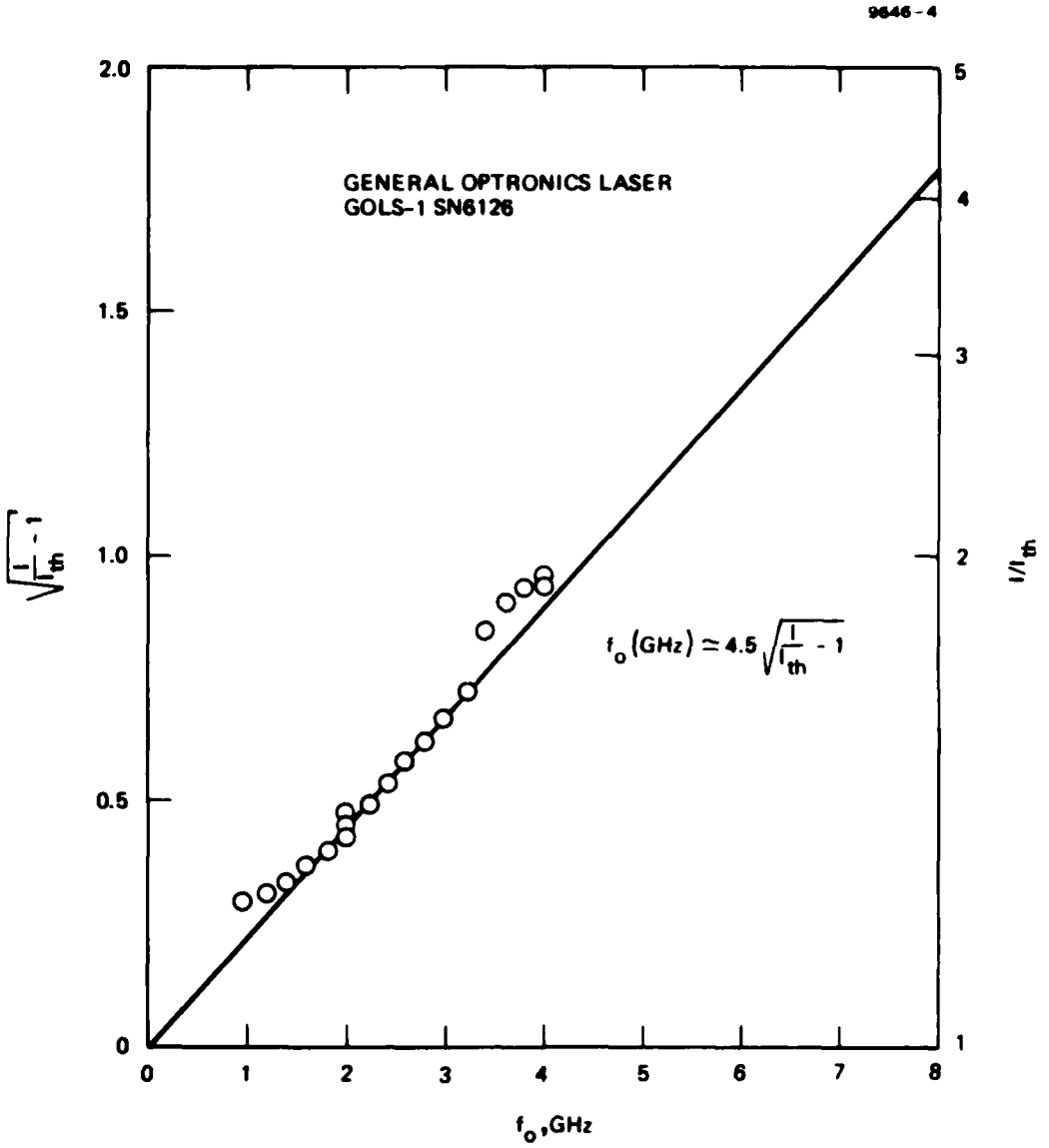

Figure 18. Relaxation oscillation frequency as a function of bias for the General Optronics laser.

SECTION 3

HIGH SPEED OPTICAL DETECTORS

This section describes our work on the characterization of commercial high-speed optical detectors and GaAs MESFET detectors. This work, when combined with our previous study of novel GaAs/(GaAl)As waveguide detectors, provides a comprehensive evaluation of high-speed optical detectors. The realization of microwave-optical systems will require optical detectors that can respond to frequencies beyond 10 GHz. Thus, a thorough characterization of existing commercial and new optical detectors is essential. This effort can lead to the optimization of detector parameters, which will enable operation at frequencies beyond 10 GHz.

A. COMMERCIAL P-N JUNCTION DETECTORS

Table 2 is a list of the various commercial p-n junction detectors characterized. The rise and fall times of the detector are basically determined by the $R_L C_j$ time and the carrier transit time. Figure 19 is an idealized equivalent circuit of the detector and the load resistance R_L presented to it. R_j is the reverse-biased junction resistance (typically in excess of 1 MΩ), C_j is the depletion capacitance, R_S is the series or spreading resistance of the junction, L_S is the inductance of the bond wire, and i_{ph} is the photocurrent. Stray capacitance of the amplifier and load have been neglected. If i_{ph} were an impulse (i.e., $i_{ph} = Q_o \delta(t)$, where $\delta(t)$ is the Dirac delta function), the current through the load (neglecting transit-time effects and assuming R_S and L_S to be small) would be

$$i_L(t) = \frac{Q_o}{R_L C_j} S(t) \exp - \left(\frac{t}{R_L C_j}\right) , \qquad (11)$$

Table 2. HRL Response Time Measurements[a] of Various Commercial Picosecond Photodetectors

Manufacturer and Model Number	Type	Material	Spectral Sensitivity,[b] nm	Quantum Efficiency[b]	Active Area cm^2	t_r,[a] psec	t_f,[b] psec	Comments on Response Time
1. Mitsubishi PD1202B	APD	Si	500 to 900	~20% @800 nm	3×10^{-4}	~130	~700	Independent of focusing
2. NEC NDL2102	PIN	Si	500 to 1100	~60% @830 nm	3×10^{-4}	~140	~800	t_f depends on focusing
3. Opto-Electronics PD 10-01	PIN	Si	300 to 1100	~23% @820 nm	2.5×10^{-3}	~130	~130	Insensitive to focusing, ringing in "back porch"
4. Opto-Electronics PD 10-02 (W. Optical Fiber)	PIN	Si	300 to 1100	~23% @820 nm	2.5×10^{-3}	~100	~160	~100 psec flat top observed; detector essentially identical to PD 10-01
5. Spectra-Phys. 403B	Micro-wave PN junction	Si	250 to 1060	Not Specified	Annular region, ~90 μm diameter metalization	~50	~80	Very sensitive to focusing, ringing in "back porch"
6. Telefunken BPW28	APD	Si	450 to 950	~80% @600 nm	3×10^{-4}	~100	~140	Independent of focusing
7. Telefunken S171P	APD	Si	450 to 950	~80% @600 nm	3×10^{-4}	~80	~140	Identical to BPW28, except for mounting
8. Texas Instr. TIED 55	APD	Si	500 to 1000	~50% @800 nm	5×10^{-4}	~100	~400	Independent of focusing
9. Rockwell	APD	GaAs GaAl/As	600 to 900	≥50% @820 nm	1.6×10^{-5}	60	<100	Very sensitive to focusing

[a] Rise and fall times measured with ~5 psec coherent dye laser pulses @ 570 nm, including the response of the Tektronix S4 sampling head (t_r < 25 psec).

[b] Data specified by manufacturer; quantum efficiency specified without avalanche gain.

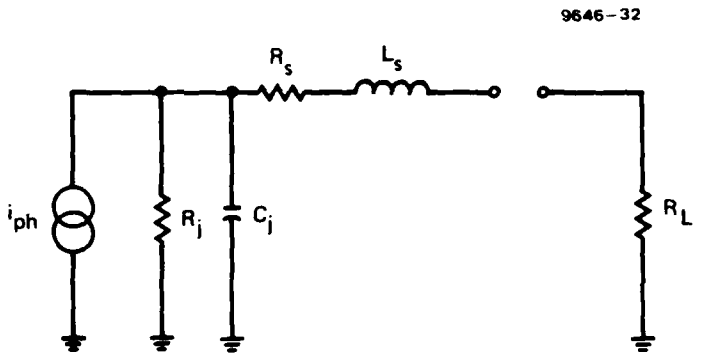

Figure 19. Equivalent circuit for the detector.

where S(t) is a step function (=0 for $t < 0$, =1 for $t > 0$), and Q_o is the total charge of photocarriers collected in the pulse. The decay time (90% to 10%) due to RC effects is then

$$t_{f,RC}(90\% \text{ to } 10\%) = 2.2\ R_L C_j \simeq 100 \text{ psec}$$

for $R_L \simeq 50\ \Omega$ and $C_j \simeq 1$ pF.

Transit time effects tend to smear the pulse width. If the incident light pulse is $P_o\delta(t)$, the current response (neglecting parasitics) will be

$$i_{ph}(t) = \begin{cases} \frac{q\eta}{h\nu} \frac{P_o}{\tau} M & 0 < t < \tau \\ 0 & \text{otherwise,} \end{cases} \tag{12}$$

where η is the detector quantum efficiency (carriers collected per incident photon), $h\nu$ is the photon energy, τ is the carrier transit time, and M is the photocarrier multiplication (M = 1 for a PIN). The transit time is given by

$$\tau = \frac{W}{v} \quad , \tag{13}$$

where W is the width of the depletion region, and v is the carrier velocity. For high fields (i.e., $E > 10^5$ V/cm), v saturates at 10^7 cm/sec for holes and electrons in GaAs, Ge, and Si. For a depletion region of 10 μm, $\tau \simeq 100$ psec. Thus, the transit and RC times are roughly comparable for commercial high-speed detectors. Figure 20 shows the magnitude and phase response of the detector due to transit-time effects.

B. DETECTOR BANDWIDTH FOR ANALOG SYSTEM

The detector bandwidth is closely related to its response time. If the optical power is sinusoidally modulated as

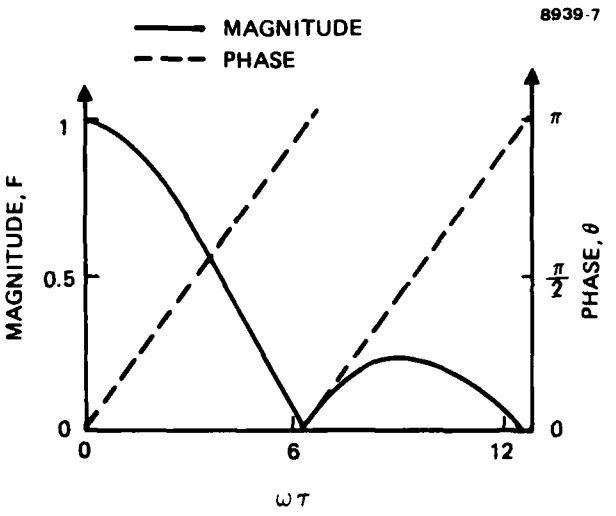

Figure 20. Phase and magnitude of the transit-time response.

$$P = P_o(1 + me^{j\omega t}) \quad , \tag{14}$$

the photodetector response will be

$$i_{ph}(t) = \frac{q\eta}{h\nu} P_o M \left[1 + me^{j\omega t} \left(\frac{1 - e^{-j\omega\tau}}{j\omega\tau}\right)\right] \quad , \tag{15}$$

and the current delivered to the load R_L (assuming only the shunt capacitance C_j) will be

$$i_L(t) = \frac{q\eta}{h\nu} P_o M \left[1 + me^{j\omega t} \left(\frac{1 - e^{-j\omega\tau}}{j\omega\tau(1 + j\omega R_L C_j)}\right)\right] \quad . \tag{16}$$

If the detector is RC limited, the power delivered to the load will have a 3-dB bandwidth of

$$f_{RC} = \frac{1}{2\pi R_L C_j} \quad . \tag{17}$$

For $R_L = 50\ \Omega$, C_j must be 0.5 pF or less to obtain a bandwidth in excess of 6 GHz. R_L can be decreased, but the effects of R_S become more significant as this is done. The -3 dB power point for a transit-time-limited detector is

$$f_\tau = \frac{0.45}{\tau} \quad . \tag{18}$$

For a 6-GHz bandwidth, the transit time must be 75 psec or less.

If the detector response can be modeled as $e^{-t/\tau}$ for $t > 0$, then the -3 dB power point will be

$$f_{-3\ dB} \simeq \frac{0.35}{t_f} \quad , \tag{19}$$

where $t_f = 2.2\ \tau$ is the 90% to 10% fall time. In this case, $t_f \leq 60$ psec for a 6-GHz bandwidth. If the detector is more accurately modeled by a Gaussian pulse response (i.e., e^{-t^2/τ^2} for all t), the -3 dB power point will be

$$f_{-3\ dB} \simeq \frac{0.22}{t_r} \quad , \tag{20}$$

where t_r is the 10% to 90% rise or fall time and must be 35 psec or less for a 6-GHz bandwidth. The data in Table 2 show that the maximum $f_{-3\ dB}$ frequency as given by Eq. 19 is ∿7 GHz for the Spectral Physics detector. The minimum $f_{-3\ dB}$ frequency is ∿2.5 GHz for the NEC PIN device. Our preliminary conclusion is that commercial p-n junction detectors operating in the spectral range 0.5 to 0.9 μm can only provide efficient sensitivity for frequencies up to 7 GHz in analog systems and can respond to pulses with 50 to 100 psec half-widths in digital systems.

C. GaAs MESFET OPTICAL DETECTORS

This subsection describes our work on the high-frequency optical characterization of various GaAs MESFETs. This work was undertaken after our initial results on the sensitivity of GaAs/(GaAl)As waveguide MESFET detectors[2] suggested that using conventional shorter-gate GaAs MESFETs would improve performance. Our measurements suggest that the mechanism responsible for the optical response of a GaAs MESFET is photoconductivity; this is in agreement with the experimental results of

Gammel and Ballantine.[3] Thus, the analog response of the MESFET can be expressed as

$$\Delta I'_{DS}(f) = (C)(P_{in}) \left(\frac{\tau}{\tau_{tr}}\right)\left(\frac{1}{1 + (\omega\tau)^2}\right)^{1/2} , \qquad (21)$$

where

$\Delta I_{DS}(f)$ is the detected rf drain-source current

C is a constant which can be fit from experiment

P_{in} is the incident power

τ is the lifetime of the slower injected carrier (holes in this case)

τ_{tr} is the transit time of the faster carrier (electrons in this case)

$\omega = 2\pi f$, where f is the frequency of the modulated incident light.

In Eq. 21, all of the parameters except τ can either be calculated or determined from experiment. The only difficult problem is to calculate the hole lifetime. In our modeling, we assumed that the hole lifetime is primarily determined by surface recombination. This assumption should be valid in GaAs MESFETs without a passivating layer since the surface recombination of a free GaAs surface can be quite high.[4] Furthermore, the amount of surface recombination is a function of the electric field present within the recombination region[5] and thus is a function of the applied gate voltage. The following simple relationship between hole lifetime and surface recombination has been derived by Wang:[5]

$$\frac{1}{\tau} = \frac{1}{\tau_b} + \frac{V_s}{d^\tau} , \qquad (22)$$

where τ_b is the bulk lifetime, V_s is the surface recombination velocity, and d' is the effective thickness of the recombination region. The value of d' ranges from d to $1/\alpha$, where d is the thickness of the FET active region, and α is the attenuation coefficient of the incident light. If we assume a very high surface recombination velocity, then Eq. 22 reduces to

$$\frac{1}{\tau} = \frac{V_s}{d'} \quad . \tag{23}$$

Since the value of d' is difficult to determine, we will assume it to be an adjustable parameter that can be obtained from the measurements. However, only those carriers generated within the high electric field active region can contribute to the high frequency response. This implies that the active region thickness is approximately equal to d'. Thus, the problem simplifies to the calculation of the surface recombination velocity. The simplest expression for the surface recombination velocity is given by

$$V_s = \frac{V_s'}{\cosh\left[\dfrac{q\,(V_t - \gamma\,(|V_g| + V_{bi})}{kT}\right]} \qquad |V_g| < V_p \tag{24}$$

$$= \frac{V_s'}{\cosh\, q\left[\dfrac{V_t - \gamma\,(|V_p| + V_{bi})}{kT}\right]} \qquad |V_g| \geq V_p \quad ,$$

where V_p is the pinch-off voltage, and the surface potential is assumed to be altered by the applied gate voltage, which in turn affects the surface recombination velocity. The voltage V_t is a constant, characteristic of the type of surface, and V_{bi} is the built-in voltage. The factor γ is a geometrical factor that takes into account that the voltage at the position where the holes recombine is not equal to the applied gate voltage but is related to the fringing of the voltage around the gate electrode. To simplify the algebra, we assume $V_t \gg \gamma(V_g + V_{bi})$

since we expect γ to be small and V_t is assumed to be the voltage due to a midgap state ($V_t \simeq 0.7$ eV). Eq. 24 reduces to

$$V_s = V_{so} \exp\left\{\frac{\gamma(|V_g| + V_{bi})}{kT}\right\} \quad |V_G| < V_p$$

$$= V_{so} \exp\left\{\frac{\gamma(|V_p| + V_{bi})}{kT}\right\} \quad |V_G| \geq V_p \quad , \tag{25}$$

where kT is the thermal energy (0.026 eV for T = 300°K), and V_{so} is the surface recombination velocity for $|V_g| + V_{bi} = 0$. The value of V_{so} is assumed to be known.[4] The parameter γ can be determined from the experimental ΔI_{DS} versus V_{GS} data and is given by

$$\gamma = \frac{\left(\frac{KT}{q}\right) \ln\left(\frac{\Delta I_{DS_2}}{\Delta I_{DS_1}}\right)}{\left[V_{GS_1} - V_{GS_2}\right]} \quad . \tag{26}$$

Figure 21 shows the variation of detected drain source current ΔI_{DS} versus gate-source voltage $|V_{gs}|$ under dc conditions. The dashed line represents a theoretical fit using Eqs. 21 and 25; the fit is excellent. Note the large detected currents (ΔI_{DS} as high as 20 mA) with only a maximum of 0.9 mW laser optical power. The input power to the GaAs MESFET is actually much less since we expect poor optical coupling to the active region. We believe the large dc response is due to traps at the interfaces of the active region. To better see how the theory predicts the optical response, the detected rf current $\Delta I'_{DS}$ (f = 2 GHz) is plotted versus $|V_{GS}|$ in Figure 22 for two different types of GaAs MESFETs. The dashed curve is a theoretical fit. The agreement between theory and experiment appears to be adequate over a certain range of frequencies.

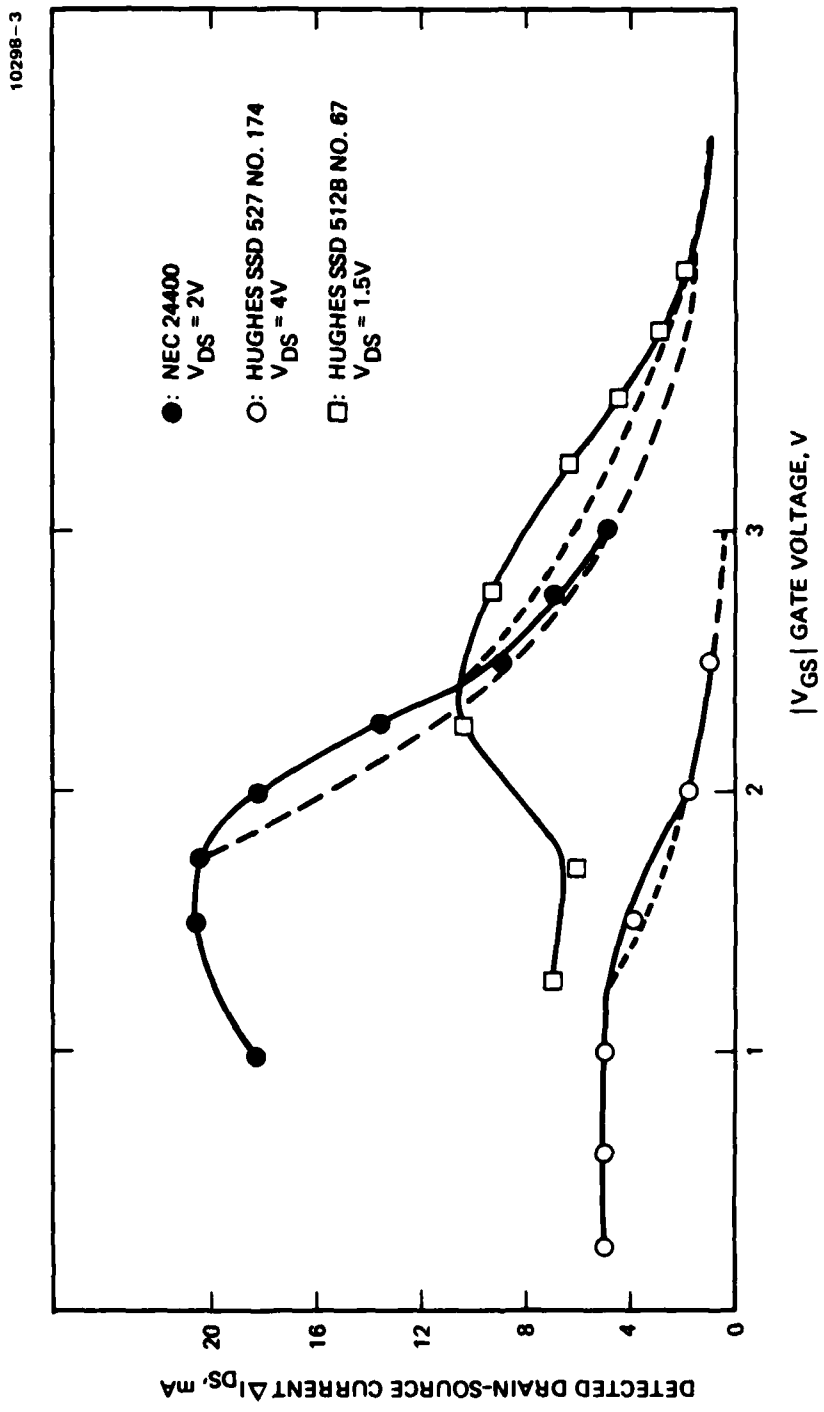

Figure 21. Detected dc drain-source current (ΔI_{DS}) versus gate voltage (V_{GS}). (The incident optical power is ~0.9 mW).

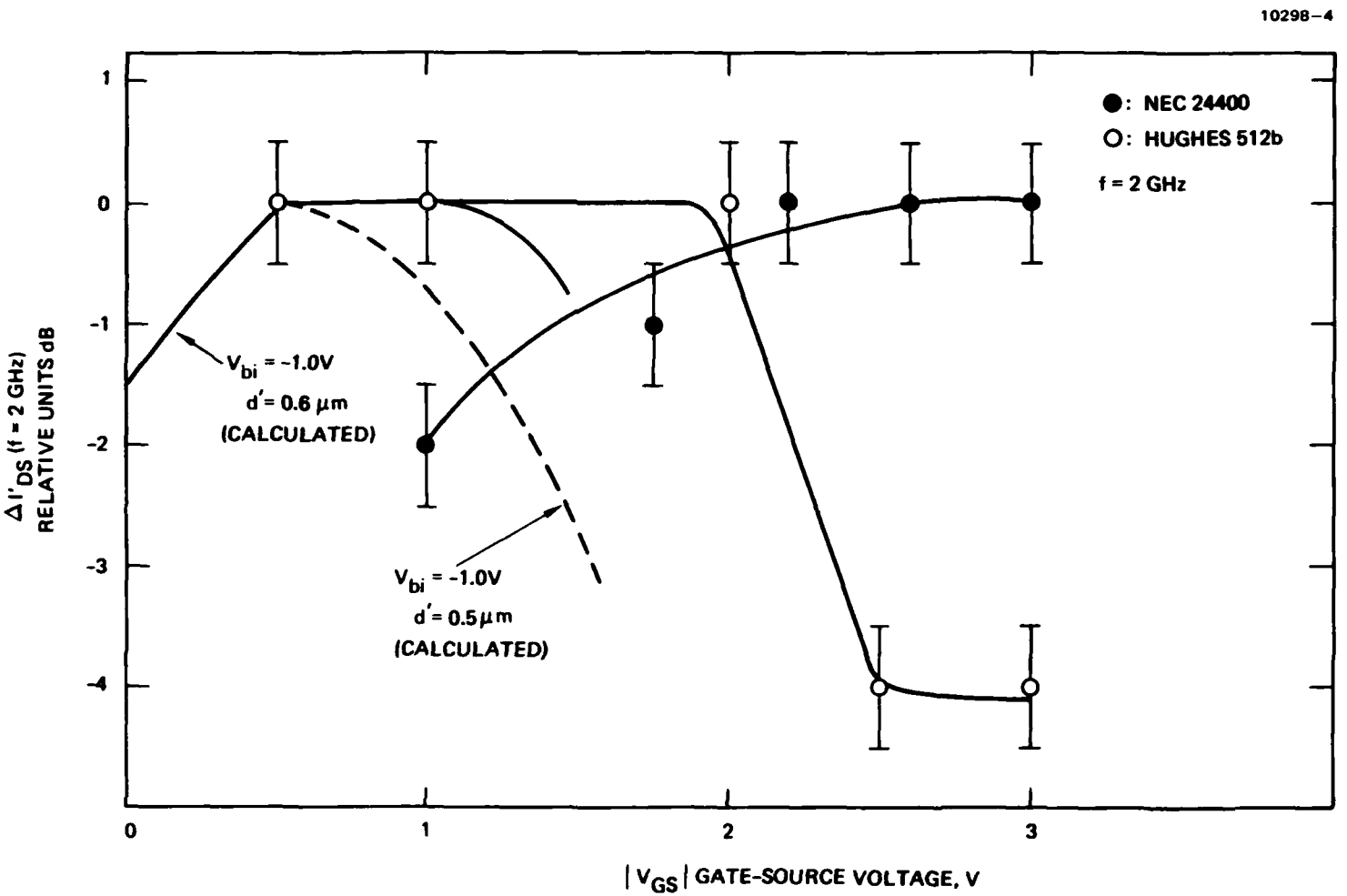

Figure 22. Detected rf drain-source current ($\Delta I'_{DS}$(f = 2 x 10^9/sec) versus gate voltage (V_{GS}).

Table 3 summarizes the results for the parameters used for the theoretical fit. We have also measured the analog frequency response of GaAs MESFETs by shining a modulated GaAs laser beam on the active region. We found that the frequency response is essentially flat for frequencies up to ∿4 GHz. Furthermore, the sensitivity is comparable to the Rockwell detector described in Table 2. Figure 23 shows the optical pulse response of typical GaAs MESFETs; the pertinent data are summarized in Table 4. Typical rise times are less than 100 psec, and the 0.5-μm HAC MESFET can detect a pulse of ∿80 psec halfwidth. The 1/2-μm-gate-length MESFET appears to be faster than the 1-μm-gate-length device, as determined from the measured pulse width. However, the measurements are somewhat obscured by the relatively large amount of trigger jitter present. In light of our theoretical calculations, it might appear difficult to see why a 1/2-μm-gate-length MESFET will be faster than a MESFET with a 1-μm-gate-length since the rise-time is determined by the recombination time. However, the recombination time (as discussed above)

Table 3. Summary of MESFET Detector Parameters

Device	γ	d'(μ), μm	d(μ), μm
Hughes FET SSD 512b	0.0271	0.5	0.2 to 0.3
Hughes FET SSD 527b	0.0321	0.5	0.2 to 0.3
NEC 24400	0.0290	0.6	0.2

$V_{so} = 1 \times 10^{5}$ cm/sec

$\tau_{tr} = 4 \times 10^{-12}$ sec (assuming $L_G = 1$ μm, and $V_e = 2 \times 10^{7}$ cm/sec)

$V_{bi} = -1.0$ V

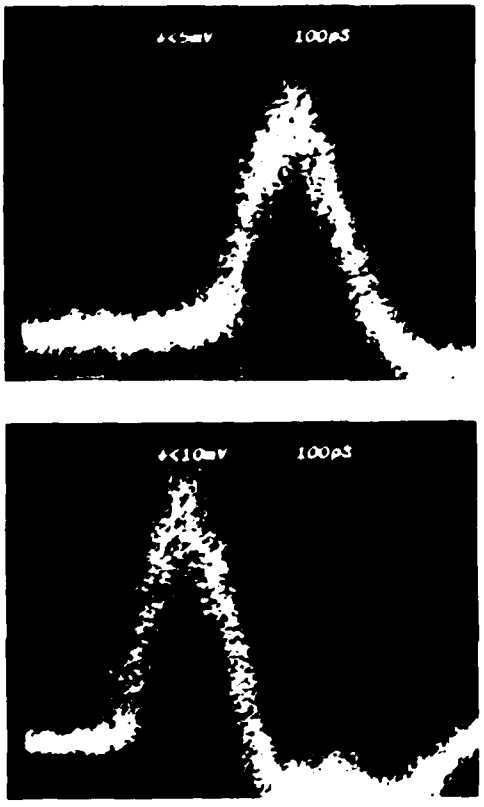

Figure 23. Optical pulse response for a HAC GaAs MESFET. (a) 1 μm gatelength, (b) 1/2 μm gatelength.

Table 4. Summary of Important Detector Parameters for Various GaAs MESFETs

Device Model Number	Type	Material	Spectral Sensitivity (η), μm	Quantum Efficiency	Active Area, cm^2	t_r, psec	t_f, psec	f_{-3dB}, GHz	Comments
HRL FET SSD 512B	Power FET	GaAs	$\lambda < 900$	-	2 μm x 580 μm regions on either side of the 1 μm gate	<100	150	≥ 3.5[a]	Fill time difficult to measure due to ringing in the package
HRL FET L 157	Low-Noise FET	GaAs	$\lambda < 900$	-	2 μm x 580 μm regions on either side of the 1/2 μm gate	<100	150	≥ 7[b]	Fill time difficult to measure due to ringing in the package
NEC FET 24400	Low-Noise FET	GaAs	$\lambda < 900$	-	Two 1.5 μm x 150 μm regions on either side of 1 μm gate	<100	150	≥ 3.5[a]	Fill time difficult to measure due to ringing in the package

[a] Measured using a modulated (GaAl) as laser.

[b] Calculated using Eq. 19 and assuming t_f = 50 psec.

is a strong function of the surface recombination velocity, the applied field, and the thickness of the active region. Thus, the result does not appear inconsistent with our theoretical formulation.

The encouraging results obtained with the GaAs MESFETs indicate that a photoconductive detector can provide a very large frequency bandwidth (potentially greater than 10 GHz) with reasonable sensitivities. To increase the sensitivity of the detector, we must modify the geometry of the device by using an interdigital structure. The device speed can be increased by reducing the electrode spacing and modifying the electrode structure to optimize the electric field where carriers recombine. Minimizing traps at the various active region interfaces can reduce the anomalous low-frequency sensitivity.

SECTION 4

STUDY OF MODE-LOCKING IN (GaAl)As INJECTION LASERS

This section describes the important parameters affecting the mode-locking of (GaAl)As injection lasers operating in an external optical cavity. In particular, we describe the characteristics of both single- and multilongitudinal-mode lasers from a variety of commercial manufacturers. We have characterized both self-pulsing and nonpulsing injection lasers, and our results indicate that "good" mode locking (pulses with 100% modulation depth and less than 200 psec pulse width) can only be obtained in lasers having either a narrow-band noise resonance or self-pulsations and operating at current below that necessary to induce the sharp resonances in the isolated laser. Furthermore, the amplitude, pulse width, and frequency of the mode-locked pulses are a strong function of the external cavity length and laser current. Lastly, we have successfully mode locked an injection laser and time multiplexed the light output to produce pulses with ∿2-GHz repetition rate.

A. EXPERIMENTAL SET-UP AND DC CHARACTERISTICS

Figure 24 shows the experimental arrangement for the external cavity geometry. We have used several different types of commercial (GaAl)As stripe geometry lasers, and their important characteristics are summarized in Table 5. All of the lasers operate cw at all times.

The external resonator consisted of a 40X microscope objective and a flat mirror. The experimental arrangement has the laser mounted at the end of a microstrip bias tee with a 47-Ω resistor placed in series with the rf input to provide impedance matching. The external cavity was aligned by collimating the output beam from one facet of the laser and adjusting the return beam so as to increase the laser output from the other facet. The final alignment was accomplished using PZT-controlled micrometers. The light output from the second facet of the laser was collected and focused onto a Si avalanche diode (Telefunken

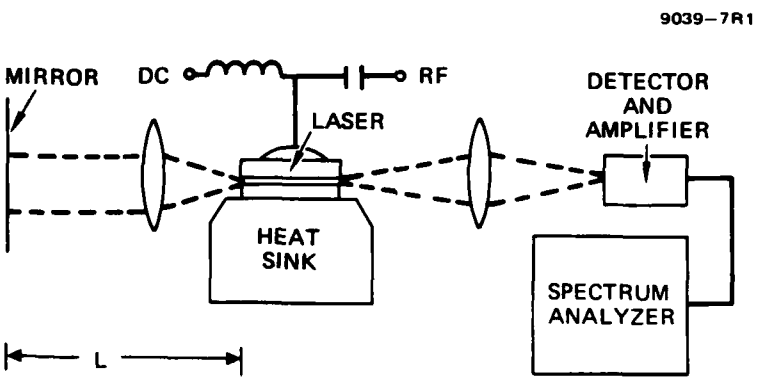

Figure 24. Experimental set-up graphically displaying the external cavity arrangement.

Table 5. Summary of Laser Structures Used in the Experiments[a]

Laser Type	Longitudinal Modes (spectral width)	Threshold Current, mA	Dynamic Characteristics	Label	Number of Lasers Tested
Buried heterostructure (BH) Hitachi	Single ($\Delta\lambda_{1/2} \leq 3$ Å)	20	Non-Pulsing	BH-NP	1
Buried heterostructure (BH) Hitachi	Multimode ($\Delta\lambda_{1/2} > 40$ Å)	29, 30	Narrow band noise resonance (NR)	BH-SP	2
Channel substrate planar (CSP) Hitachi	Single ($\Delta\lambda_{1/2} \leq 3$ Å)	60, 75	Non-Pulsing	CSP-NP	2
Channel substrate planar (CSP) Hitachi	Multimode ($\Delta\lambda_{1/2} < 10$ Å)	90	NR	CSP-SP	1
Constricted double heterostructure (CDH) RCA	Multimode ($\Delta\lambda_{1/2} < 15$ Å)	75 to 80	Non-Pulsing	M-CDH-NP	3
Constricted double heterostructure (CDH) RCA	Single ($\Delta\lambda_{1/2} \leq 3$ Å)	80 to 85	Non-Pulsing	S-CDH-NP	5
General Optronics stripe (G.O.)	Multimode ($\Delta\lambda_{1/2} < 10$ Å)	60 to 100	NR	G.O-SP	4
General Optronics stripe (G.O.)	Multimode ($\Delta\lambda_{1/2} > 50$ Å)	60 to 100	NR and self-pulsing	G.O-SP	5

[a]All of the lasers, either with a narrow-band noise resonance or self-pulsations (except the BH), tested were specially selected by the respective manufacturers to provide the observed characteristics. The pulsing BH lasers started pulsing after operation at high power levels. We would like to emphasize that the characteristics of these specially selected lasers are not representative of the commercially available lasers provided by the above manufacturers.

model S171P) using a microscope objective. The rise and fall times of the detector were each ∿100 psec. When the light output from the laser was small, we followed the detector with a B&H amplifier having a 3.1-GHz bandwidth and 30-db gain. The rf input to the laser was provided by an HP sweep oscillator (8690B). The maximum rf power going into the laser was estimated to be less than a few milliwatts for the cases considered. The output from the avalanche diode was fed to either an HP spectrum analyzer (8565A) or a Tektronix sampling oscilloscope (S4).

Figure 25 shows typical light output versus current characteristics for different types of laser structures operating with an external resonator (ER). The lasers used are described in Table 5. For comparison, the light output characteristics with no external resonator (NER) present are also shown. An important figure of merit for a laser-external resonator combination is the threshold reduction factor[6] K, which is given by

$$K = \frac{I_{th}\ (ER)}{I_{th}\ (NER)} \quad , \tag{27}$$

where I_{th} (ER) and I_{th} (NER) are the threshold current with and without the external resonators, respectively. In a previous paper,[7] we have shown that the value of K under cw operation can be written as

$$K = \frac{\alpha_o d + (d/\Gamma)\ [\alpha_{fc} + (1/2\ell)\ \ln(1/RR_{eff})]}{\alpha_o d + (d/\Gamma)\ [\alpha_{fc} + (1/\ell)\ \ln(1/R)]} \quad , \tag{28}$$

where α_o is a loss constant, α_{fc} is the distributed loss, Γ is the transverse optical confinement factor, d is the active region thickness, ℓ is the diode length, R is the mirror reflectivity, and R_{eff} is the total fraction of light reflected back into the laser from the external and diode mirror combination. By using an R_{eff}, we are assuming a uniform photon density in the external cavity. This assumption, although

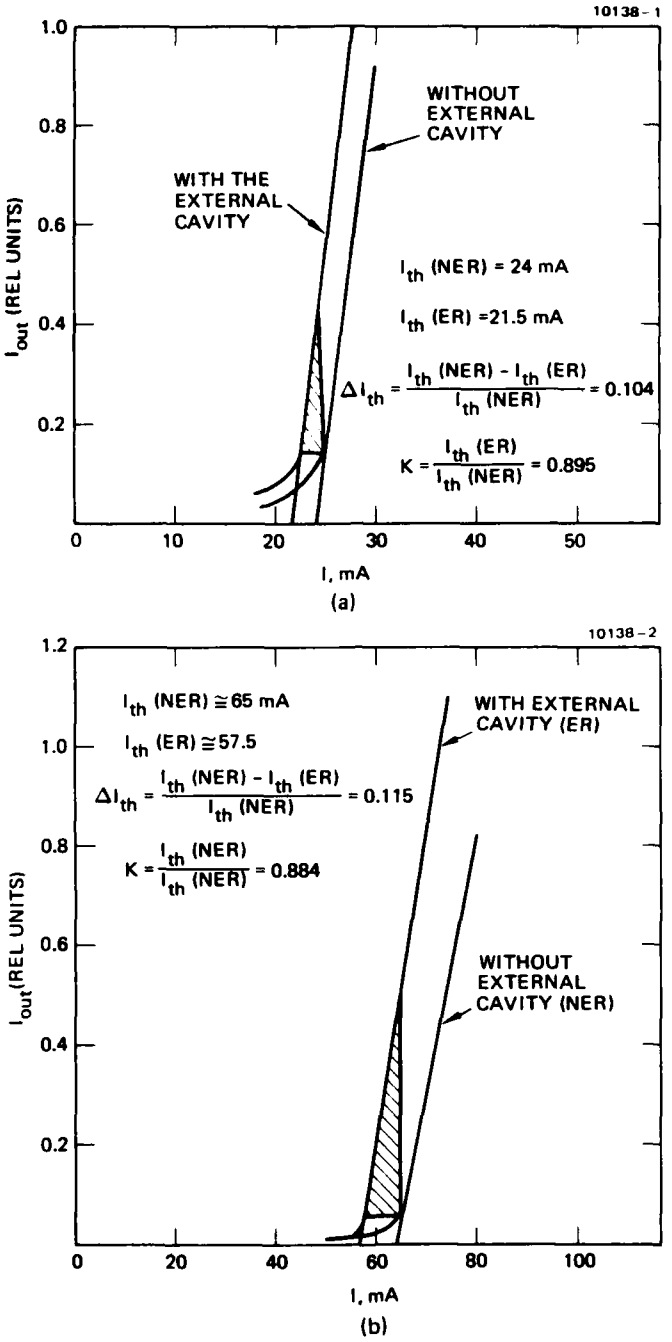

Figure 25. Experimental light output versus current characteristics, showing relatively low threshold lasers (I_{th} ∿20-30 mA) and lasers with higher threshold (I_{th} ∿60-100 mA).

adequate for cw operation, breaks down in the description of short optical pulses. The effective reflectivity R_{eff} can be written as[7]

$$R_{eff} = \frac{(\sqrt{R} + \sqrt{R_f})^2}{(1 + \sqrt{R_f \cdot R})^2} \quad , \tag{29}$$

where R_f is the light reflected from the external mirror that reaches the diode. Figure 25 shows K to be $\sim$0.1. Substituting typical values for the diode parameters ($\ell = 1.5 \times 10^{-2}$ cm, d = 0.3 μm, Γ = 0.8, R = 0.3, and $\alpha_{fc} = 20\ cm^{-1}$) into Eqs. 28 and 29 gives a range for R_f of from 0.1 to 0.2 when we assume that α_o lies between 100 and 200 cm^{-1} (a typical range).[7] This shows that only a small fraction of the light is returned to the laser. However, as shown below, the amount of optical feedback is more than sufficient to mode-lock the injection laser.

B. DYNAMIC CHARACTERISTICS OF INJECTION LASERS OPERATING IN AN EXTERNAL OPTICAL CAVITY

The dynamic characteristics of injection lasers operating in an external optical cavity have been discussed by many authors.[8] Broom et al.[9] obtained self-induced sinusoidal resonances at a frequency corresponding to either the inverse transit time or a harmonic of the relaxation oscillation frequency. The experimental results were explained by assuming an interaction between photons, injected carriers, and longitudinal mode effects. No account of the delayed photon feedback from the external cavity was considered. Paoli[10,11] and Ripper have characterized the operation of self-pulsing lasers operating in an external cavity. They concluded that sharp pulsations could be obtained by using either electrical or optical feedback. Pulses as short as 180 psec were obtained. Furthermore, they obtained frequency locking and jumping effects.

Several workers have recently observed a sharp pulsation of the light output when the laser was driven at the inverse transit time f_c of the external cavity.[12-18] The initial demonstrations have attributed the effect to active mode-locking and have been able to generate 20-psec-wide pulses at a 3-GHz repetition rate.[12] Just recently, Ippen et al. have demonstrated that 5-psec-wide pulses can be generated from degraded (GaAl)As injection lasers.[15] These results raise two questions: (1) what mechanism is responsible for self-pulsations in semiconductor lasers and (2) are there any relationships among self-pulsations, induced resonances, and the recent mode-locking experiments. This section comments briefly on the first question and concentrates on the latter.

Several models have been proposed to explain the origins of self-pulsations.[19-25] Most assume that self-pulsations are produced by either a saturable absorber[19-22,23] or a superlinear gain which increases with photon density. The saturable absorption can arise from nonuniform current flow and absorption centers distributed throughout the active region or localized near the laser facets. The superlinear gain can result from electron traps distributed throughout the active region, lateral mode instability, or excess laser noise. Other models, such as second-order mode-locking[26] and a recent model proposed by Casperson[27], appear less likely. There exists growing evidence that self-pulsations might be related as dark line defects[28] and mirror degradation.[29,30] In some recent experiments, Nash et al.[29] and Mizuishi et al.[30] have been able to either reduce or eliminate the effects of pulsations by using facet coatings.

These comments on the mechanism responsible for self-pulsations allow us to proceed to the second question. In a series of recent publications, we have shown that an external cavity can significantly alter the characteristics of an injection laser that contains either electron traps[7,31] or saturable absorbers.[32] Our results predict either enhancement or suppression of self-pulsations depending on the density of electron traps or saturable absorbers and the length of the external cavity. We have further

speculated that our calculations can explain many of the previous results on induced resonances and mode-locking. In this and the following sections, we provide calculations and further experimental evidence to support our speculations.

To correlate our experimental results (given in Sections 4.C and 4.D) with theory, we have used a model consisting of the conventional rate equations modified by two important parameters. First, as proposed by Copeland,[22] we assume that the injection laser contains electron traps. Second, we take the external cavity into account by using a delayed photon feedback term. Even though we use the electron trap model, we would like to emphasize that our calculations are quite general and not model dependent. This assertion was recently verified by using a saturable absorber model and obtaining very similar results to the electron model.[32] The equations describing the process are:

$$\frac{dN_e(t)}{dt} = \frac{J}{ed} - \frac{N_e(t)}{\tau_s} - AN_{ph}(t)\,[N_e(t) - N_o] + \frac{dT(t)}{dt} \tag{30}$$

$$\frac{dN_{ph}(t)}{dt} = \frac{-N_{ph}(t)}{\tau_{ph}} + AN_{ph}\,[N_e(t) - N_o] + \beta N_e(t)/\tau_s$$

$$- \sigma_o c_o N_{ph}(t)\,(T_o - T) + \frac{R_f N_{ph}^{(t-\tau)}}{\tau_{ph}'} \quad . \tag{31}$$

$$\frac{dT(t)}{dt} = \sigma_o c_o N_{ph}(t)\,[T_o - T(t)] - \sigma_e v N_e(t) T(t) \quad , \tag{32}$$

where N_e is the electron density (in cm^{-3}), N_{ph} is the photon density (in cm^{-3}), J is the current density (in A/cm^2), e is the electronic charge (in C), and d is the thickness of the active region (in cm). The first two equations with the exception of the last terms (those involving T and R_f) are the conventional rate equations. The effects of transverse optical confinement and current spreading are neglected. The term $(R_f N_{ph}^{(t-\tau)}/\tau_{ph}'$ represents the delayed feedback from the external

mirror, where τ, the round-trip time in the external cavity, is given by $1/f_c = \tau = 2L/c_o$, where L is the external cavity length, and c_o is the speed of light in vacuum; τ'_{ph} is the photon lifetime related to the mirror loss only and is given by $\tau'_{ph} = (c_o/nL)\ln(1/R)$, where n is the index of GaAs; R_f is the amount of light fed back into the laser. Eq. 32 represents the equation of motion for the electron traps, T is the density of empty traps, T_o is the total density of traps, σ_e is the electron capture cross section, v is the thermal velocity, and σ_o is the photon capture cross section by a trap occupied by an electron. For the calculations, we use: $A = 1.5 \times 10^{-6}$ cm^3/sec, $\tau_s = 3 \times 10^{-9}$ sec, $\tau_{ph} = 2.9 \times 10^{-12}$ sec, $d = 1 \times 10^{-4}$ cm, $N_o = 5 \times 10^{17}$ cm^{-3}, $\beta = 10^{-4}$, $c_o = 8 \times 10^9$ cm/sec, $\sigma_e = 1.5 \times 10^{17}$, $v = 4.42 \times 10^7$ cm/sec, and $\sigma_o = 3 \times 10^{-16}$ cm^2. All the calculations were performed by integrating Eqs. 30 to 32 using the Runge-Kutta fourth-order algorithm. The system is excited with a step change in current and run until steady-state oscillation or its absence is confirmed. The important parameters affecting the pulsations are $\sigma_o T_o$, β, and τ. Increasing $\sigma_o T_o$ increases the amplitude and decreases the pulse width of the pulsations. This parameter is similar to the density of saturable absorbers in other models. Increasing β (i.e., the spontaneous emission factor) quenches the pulsations. Relatively large values of β are necessary (10^{-2} to 10^{-3}) to quench pulsations. The effect of τ is to produce a series of resonant suppression and enhancement bands depending on whether τ is small or large. Also, the above equations assume a single longitudinal mode and do not take into account the optical phase. However, the model adequately describes the process and is able to explain many of the experimental results.

Figure 26 shows the effect of an external cavity on the light output of an injection laser that does not pulse but still contains a high density of electron traps. Note that it is possible to induce pulsations, and that the amplitude and pulse width are strong functions of the actual trap density. This calculation can help explain the sharp contrast between the recent mode-locking experimental results[15] and the older

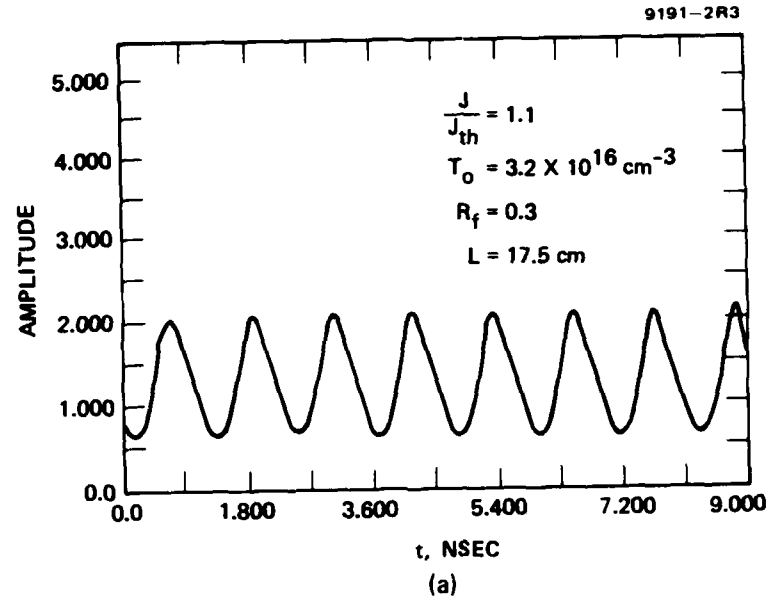

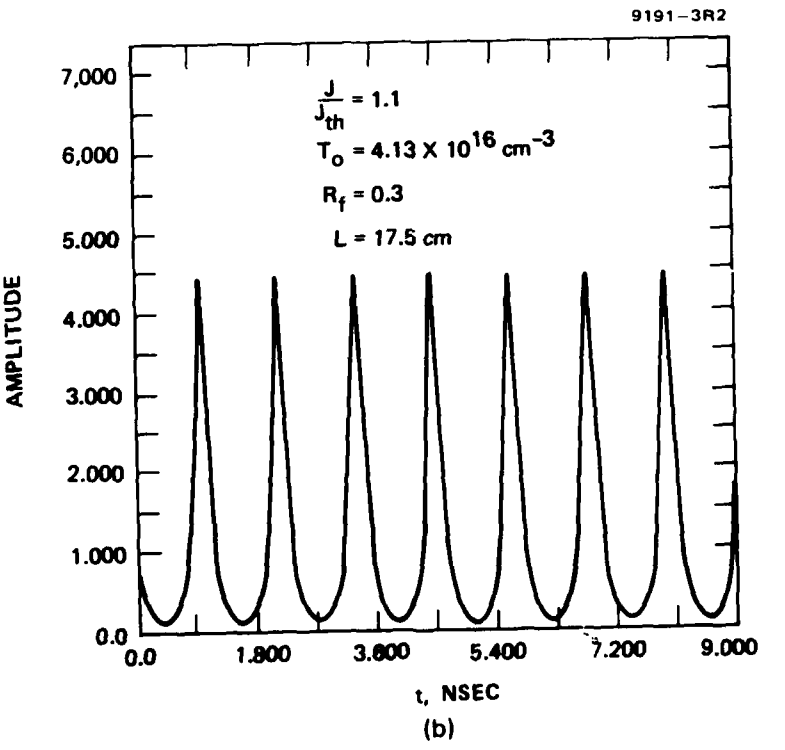

Figure 26. Calculated plot showing induced pulsations when an external cavity is aligned with a laser having a high density of electron traps.

results on induced sinusoidal oscillations.[9] Figure 27 shows the effect of varying the external cavity length on the amplitude of the induced pulsations. Note that there exists a resonant enhancement of the pulse amplitude for a cavity length of ~19 cm, and that it is possible for the pulsation to occur at $2f_c$ when the external cavity is lengthened beyond 25 cm. Figure 28 shows the variation of the induced pulse amplitude with injection current. Note that an efficient pulse output is only obtained for a small range of currents. Also, varying the external cavity length will shift the current where the maximum pulse amplitude occurs. A shift to lower current occurs when the external cavity is lengthened.

The above results can be understood qualitatively by considering two descriptions of the induced pulsation process. The first description is based on the recognition that the calculated induced pulsation is very similar to the results obtained using a passive mode-locked dye laser. Thus, some of the results applicable to the latter system should be applicable to the semiconductor laser systems. Passive mode-locking using a saturable absorber with a slow recovery time has been described by New[33] and Haus.[34] In this type of mode-locking, the saturable absorber and the laser gain act together to compress the leading and trailing edges of the circulating pulse. Several requirements must be met before such a process can produce short pulses that are much shorter than the recovery time of the saturable absorber. First, the optical cross section of the saturable absorber must be larger than the cross section for stimulated emission. This means that the absorber must be easier to saturate than the laser gain. For a semiconductor laser with electron traps, the absorber cross section is σ_o, and the stimulated emission cross section is $\sigma_L = A/c_o$. Using the numbers in Section 4.B, we find $\sigma_o/\sigma_L \sim 6$, and this requirement is easily met. The second requirement is that the relaxation time of the gain must be comparable to the pulse repetition rate. This requirement arises from the stability conditions derived by Haus, which require that the net gain of the laser system be negative after passage of the pulse.

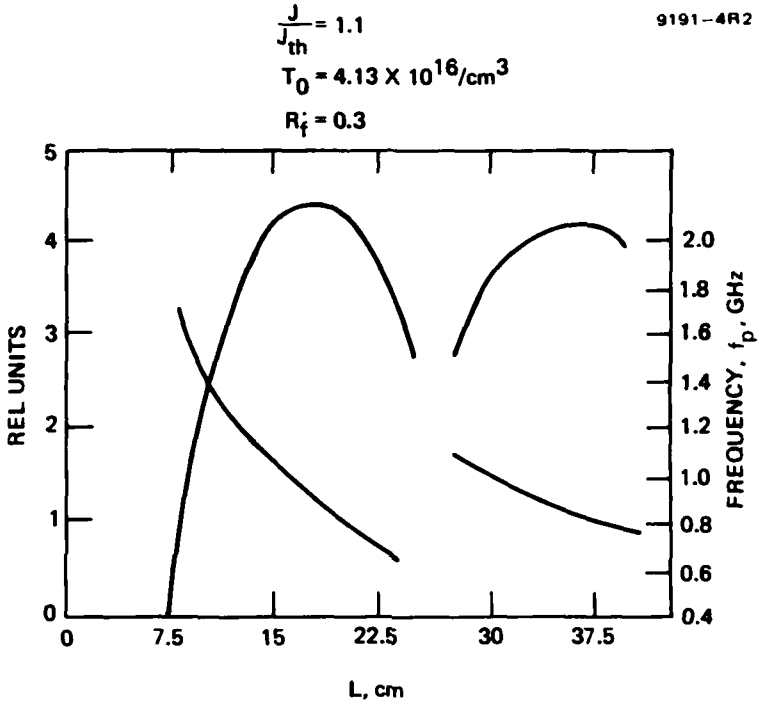

Figure 27. Calculated plot showing the variation of induced pulse amplitude versus external cavity length.

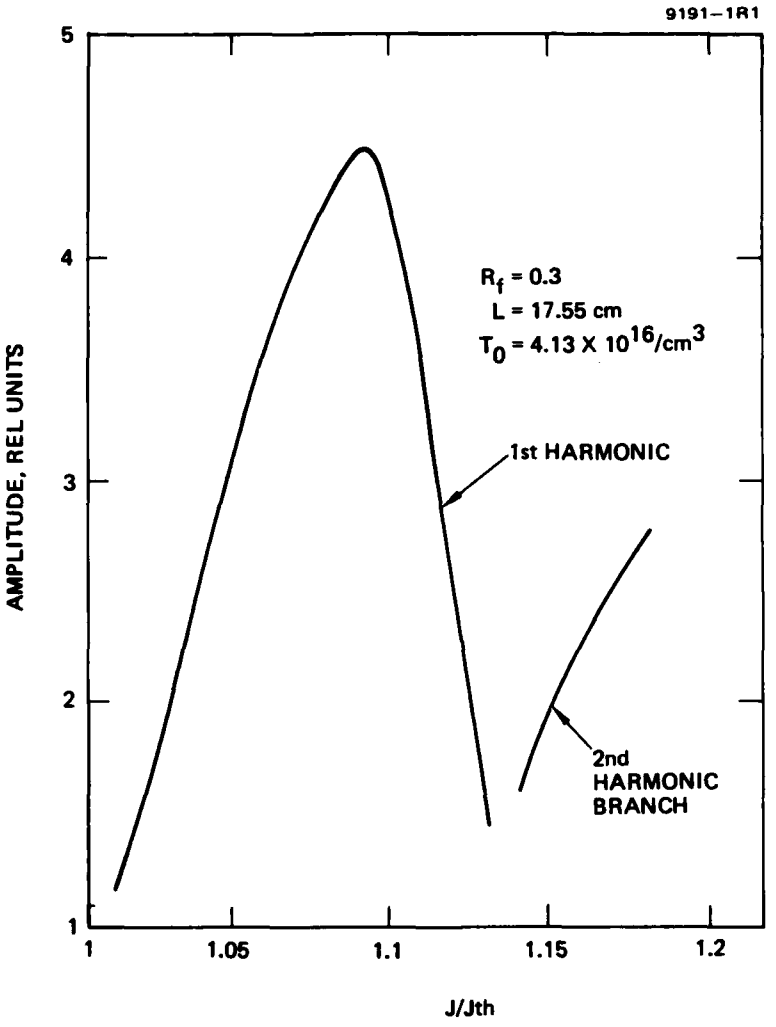

Figure 28. Calculated plot showing the variation of induced pulse amplitude versus current.

Thus, for short pulses, the gain must be shut off after the passage of the pulse. This second requirement forces us to use an external optical cavity with reasonable length in the mode-locking of the semiconductor laser systems. A typical value for the gain relaxation time τ_G is ~1 nsec (i.e., we expect $\tau_G \simeq \tau_s$), and we expect stable pulses with gigahertz repetition rates. The latter value is typical for all the reported mode-locking results. We expect that the maximum pulse-repetition frequency depends on the actual laser used, since we expect variations in the spontaneous lifetime. Lastly, the approximate analytical results derived by Haus can provide a qualitative measure of the minimum pulse width and how it varies with laser parameters. From his results, the minimum pulse width τ_{pmin} can be derived as

$$\tau_{pmin} \propto \left(\frac{Q_R}{Q_A}\right)^{-1/2} \frac{1}{\omega_c} \quad , \tag{33}$$

where $Q_{R,A}$ represents the Q of the cavity resonator and the saturable absorber. Simplifying Eq. 33 to show the effects of cavity and absorber losses yields

$$\tau_{pmin} \propto \left(\frac{\alpha_L}{\alpha_A}\right)^{1/2} \frac{1}{\omega_c} \quad , \tag{34}$$

where ω_c is the radian round-trip frequency, α_L is the laser threshold loss, and α_A is the absorber loss given by $\alpha_A \simeq \sigma_o T_o$ in the case of electron traps. Eq. 34 can help to explain qualitatively some of our calculations (e.g., the difference between Figures 26(a) and 26(b)) and can be used to predict the parameters affecting τ_{pmin}. We conclude that to minimize the pulsewidth will require increasing the density of saturable absorbers, decreasing the laser threshold losses (e.g., by using a laser with a longer cavity length and minimizing the internal losses).

Also note that Haus neglected the effect of spontaneous emission in his discussion. However, from our numerical calculations we know that a large spontaneous emission factor tends to suppress induced pulsations. This arises from the partial saturation of the absorber by the spontaneous emission. The effect of spontaneous emission can help explain why Ippen et al.[15] observed a narrowing of the pulse output when they narrowed the bandwidth of their system. Narrowing the bandwidth limits the number of longitudinal modes present and thus tends to reduce the total spontaneous emission in comparison to a laser with no bandwidth control.

A second qualitative description of the induced pulsations has been given by Lau et al.,[32] who introduced the concept of a microwave gain transfer function, $g_p(\omega)$. The function $g_p(\omega)$ describes the conditions necessary for microwave oscillations. For microwave oscillations to occur, $g_p(\omega)$ must be greater than zero over a certain frequency band. The amplitude of $g_p(\omega)$ increases with saturable absorber density and with increased optical coupling from the external cavity. Lastly, the frequency at which $g_p(\omega)$ is a maximum increases as current increases and decreases as the density of saturable absorbers increases. These observations tend to explain qualitatively the operation of an injection laser with either saturable absorbers or electron traps operating in an external cavity. If the frequency corresponding to the inverse transit time f_c or a harmonic lies within the gain line, and if the external cavity coupling is high enough so that $g_p(\omega)$ becomes positive, induced pulsations will occur. Varying either the current or the external cavity length will produce frequency shifts in either $g_p(\omega)$ or f_c and lead to changes in the amplitude of the induced pulsation.

C. EXPERIMENTAL RESULTS WITH NONPULSING SEMICONDUCTOR LASERS OPERATING IN AN EXTERNAL OPTICAL CAVITY

This section describes the characteristics of nonpulsing injection lasers operating in an external cavity. Figures 29 and 30 display typical light output versus frequency plots for various nonpulsing lasers. Several observations can be made. Every laser exhibits a relatively

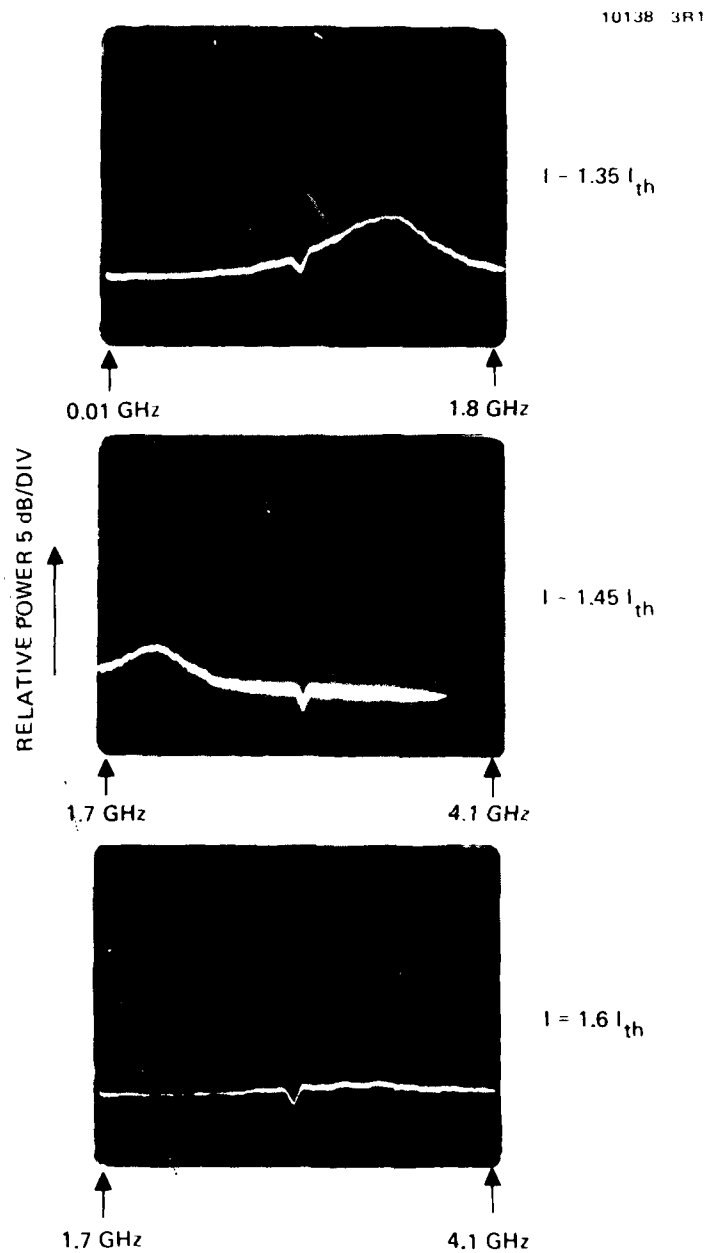

Figure 29. Experimental light output versus frequency plots for the BH-NP. The plot gives the noise frequency response versus current. No external cavity is present. Similar plots are obtained for the CSP-NP. The reader should note the relatively broad noise resonance.

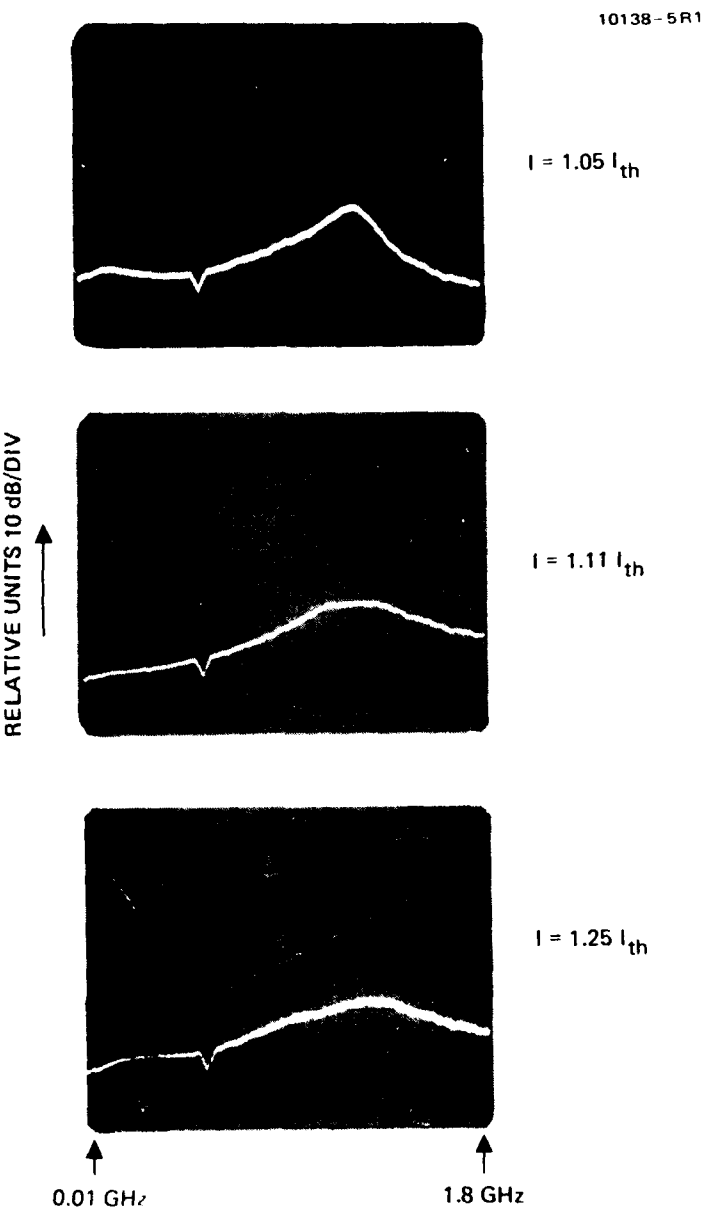

Figure 30. Experimental light output versus frequency plots for the S-CDH-NP. No external cavity is present.

broad noise resonance that occurs above 500 MHz and varies with current. In the BH-NP and the CSP-NP (not shown), the amplitude of the noise resonance decreases as current increases above threshold. This is the expected response for a well-behaved laser. For the CDH lasers, the noise resonance does not decrease as current increases and may actually increase somewhat. This last behavior is similar to that reported by Hakki[25,35] and could be related to an unsaturated mode gain. Figure 31 displays light output versus frequency plots when an external cavity is aligned with the lasers previously discussed. These photographs show that resonances corresponding to harmonics of f_c can be induced. The resonance bandwidth is typically 50 MHz. The significant low-frequency noise in single-mode lasers (S-CDH-NP, CSP-NP) broadens and destabilizes the induced resonance. The low-frequency noise is detrimental to the stabilization of the light output and to the locking action of an external rf input. We believe that the low-frequency noise is related to the longer coherence length of the single-mode laser. If we operate the lasers above the shaded region in Figure 25, the induced resonances broaden significantly ($\geq$100 MHz). To attempt to mode-lock the injection laser, an external rf signal was introduced into the laser. The frequency of the rf signal was adjusted to correspond to the inverse transit time f_c. Photographs displaying the light output are shown in Figure 32. It is clear from the figure that the pulse widths attained are relatively broad ($\tau_{p_{1/2}} \simeq$ 300 to 400 psec) except for the M-CDH-NP. The modulation depth is typically 50 to 100%. It is always possible to obtain pulsations by applying a large rf signal and operating the laser near threshold. However, this phenomenon is predicted by the conventional rate equations[36] and is produced by harmonic distortion. In this mode of operation, the pulse amplitude and pulse width are relatively insensitive to frequency (over a 100-MHz bandwidth). The short pulse widths ($\tau_{p_{1/2}}$ = 200 psec) obtained with the M-CDH-NP lead us to believe that this laser may have a high density of either saturable absorbers or electron traps. However, the density is not high enough to produce pulsations in the isolated laser. The same laser without an external

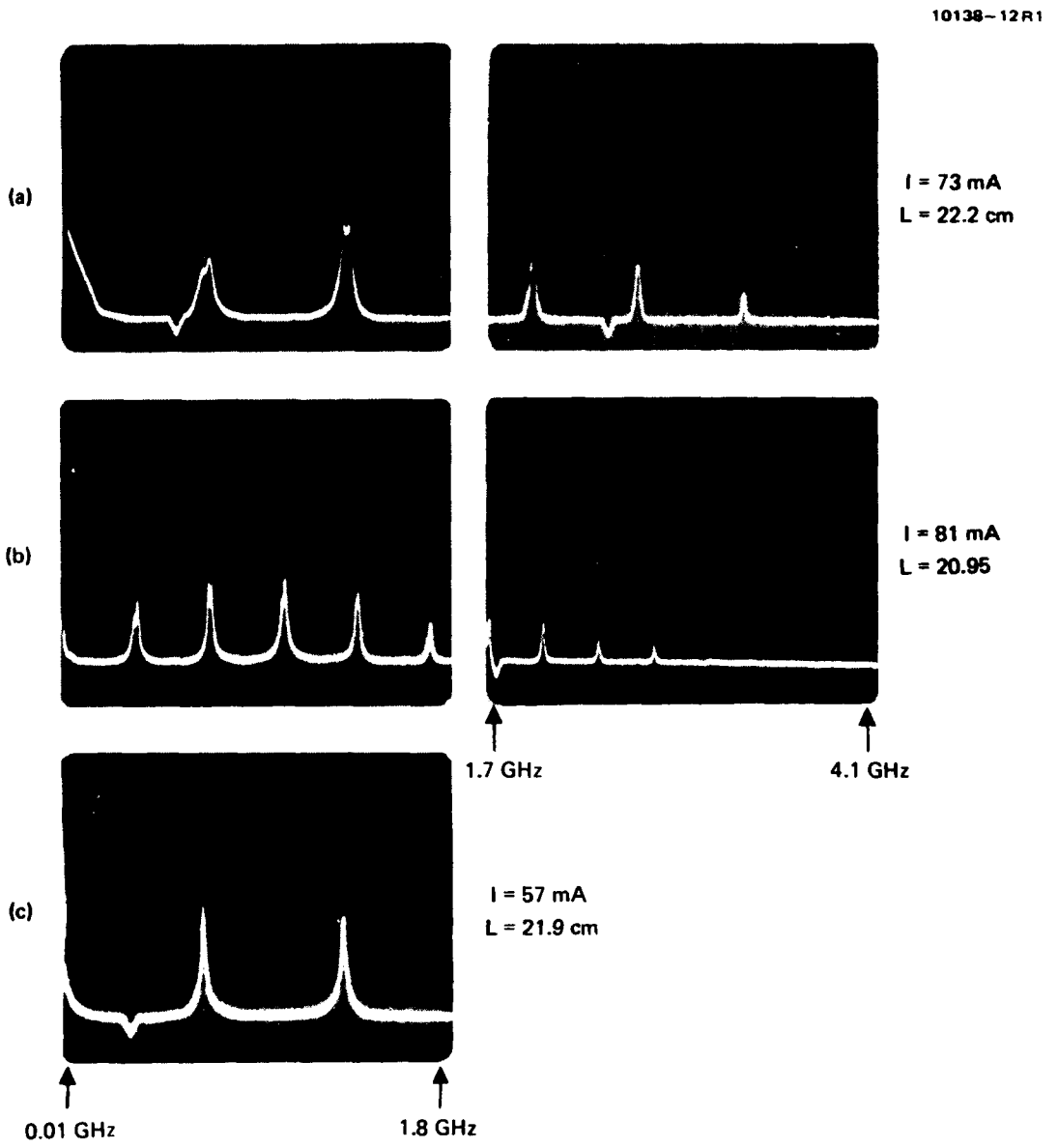

Figure 31. Experimental light output versus frequency plots when an external cavity is aligned with the lasers described in Figures 29 and 30. (a) S-CDH-NP, (b) M-CDH-NP, (c) CSP-NP.

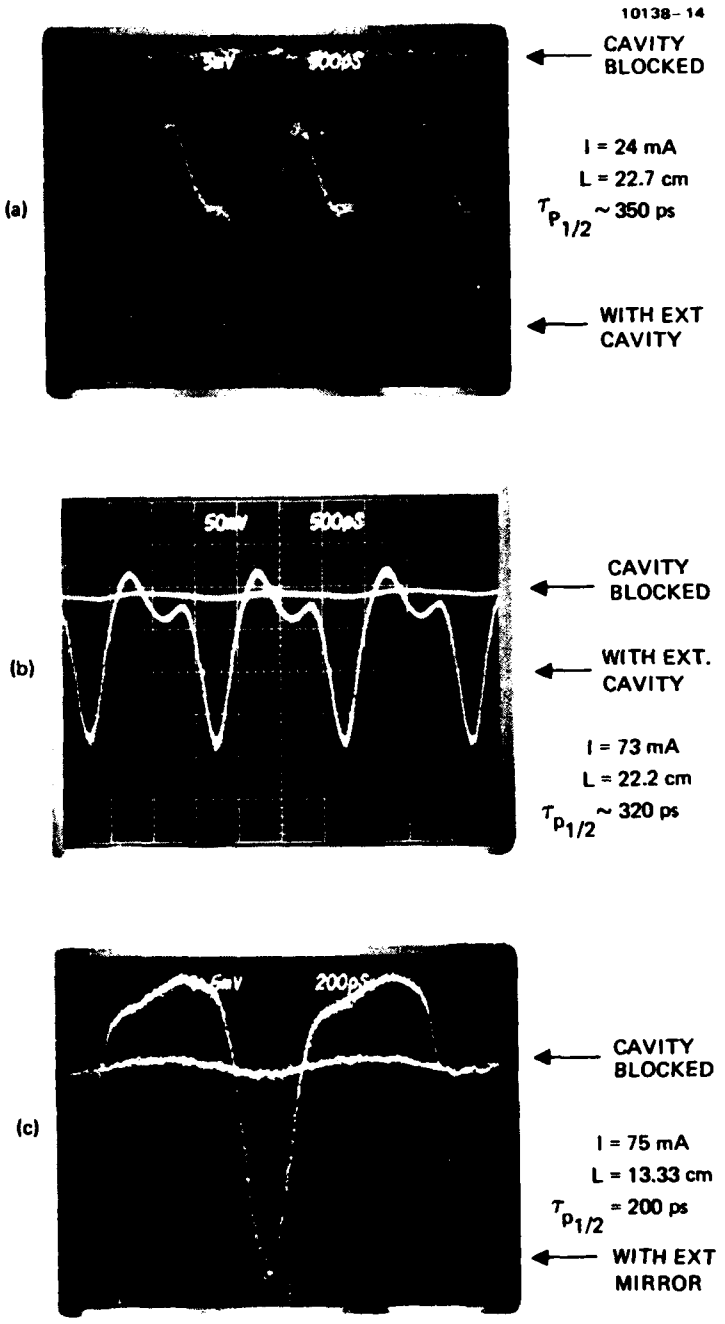

Figure 32. Experimental temporal display showing the light output when the lasers described in Figures 29 and 30 are operated in an external cavity and modulated at f_c. (a) BH-NP (similar results are obtained for the CSP-NP), (b) S-CDH-NP, (c) M-CDH-NP. (No B&H amplifier was used.)

cavity produces pulses having widths of ∿300 psec, which is lower than for any of the other non-pulsing lasers tested. It appears plausible to speculate that lasers with a high density of electron traps or saturable absorbers are more prone to emit short pulses when driven with an rf source. This should occur whether the laser actually self-pulses or not. In contrast, there appears to be some correlation between lasers with a regular frequency response (BH-NP, CSP-NP) and the inability of those lasers to emit short pulses.

D. EXPERIMENTAL RESULTS USING SEMICONDUCTOR LASERS HAVING EITHER A NARROW-BAND NOISE RESONANCE OR SELF-PULSATIONS OPERATING IN AN EXTERNAL OPTICAL CAVITY

This section describes the dynamic characteristics of lasers having either a sharp narrow-band noise resonance or self-pulsations operating in an external optical cavity. Figures 33 through 35 show typical photographs of light output versus frequency as a function of current for various types of lasers displaying sharp narrow-band resonances. The measurements were taken without an external cavity. Note the sharp resonance compared to the lasers described in Figures 29 and 30. The sharp resonance develops at a current slightly above threshold, and, in some of the lasers, the output breaks into a self-pulsation similar to that reported by previous workers.[37,38] The bandwidth of the resonance is typically less than 10 MHz, except for the CSP-SP, which has an ∿25 MHz bandwidth. When these lasers are operated in an external cavity and the current lies within the shaded region of Figure 25, we are able to induce sharp resonances at the inverse transit time f_c or a harmonic. This is shown in Figure 36. The bandwidth of the induced resonance can be less than 1 MHz, and blocking the external cavity quenches the resonance.

For the lasers described in Figure 36, we can induce a sharp pulsation of the light output when the current is modulated at the inverse transit time f_c. In some cases, a modulation of the light output occurred at $2f_c$. The frequency bandwidth for the interaction was typically a few

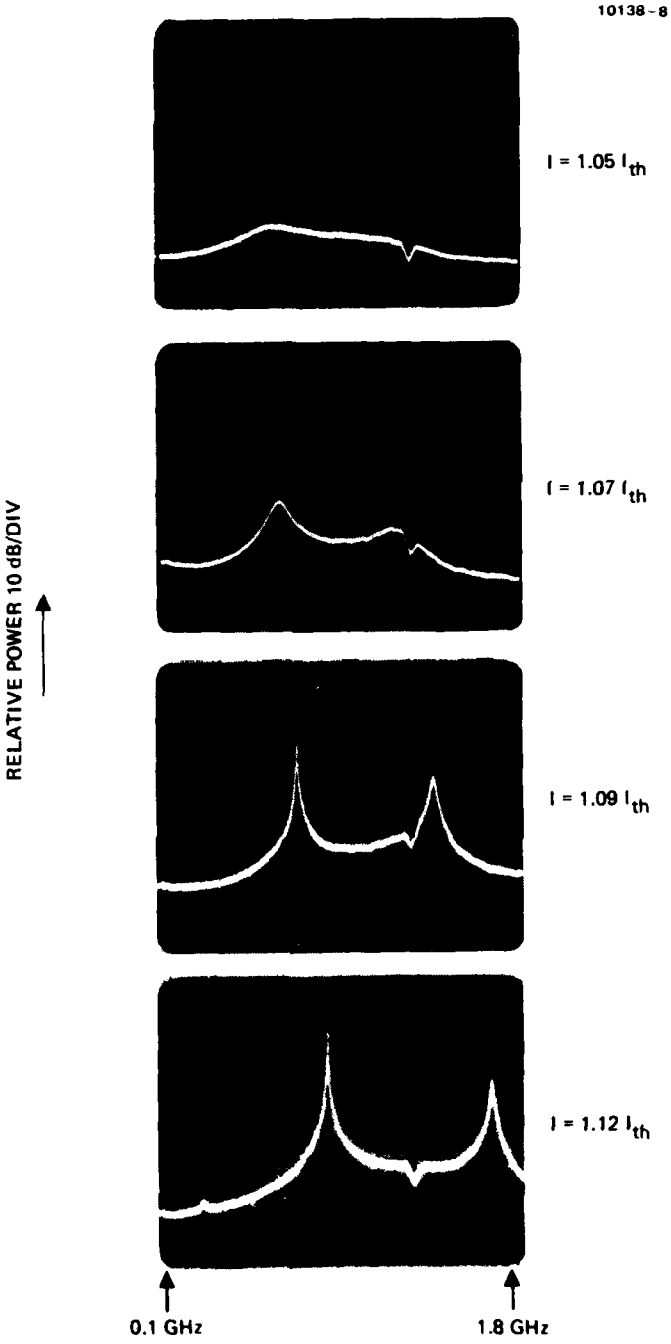

Figure 33. Experimental light output versus frequency plots for the BH-SP laser. No external cavity is present. The reader should note the relatively narrow band noise resonances.

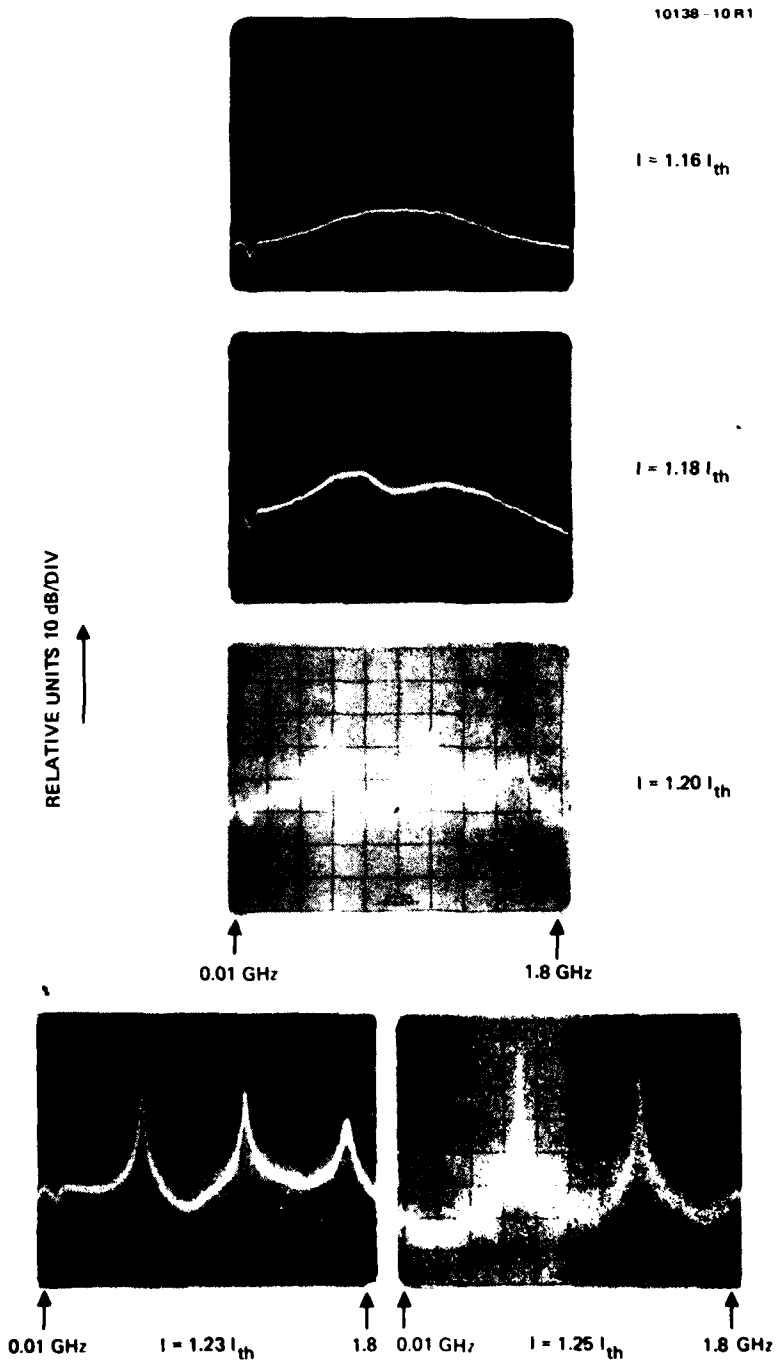

Figure 34. Experimental light output versus frequency plots for the G.O.-SP laser. No external cavity is present.

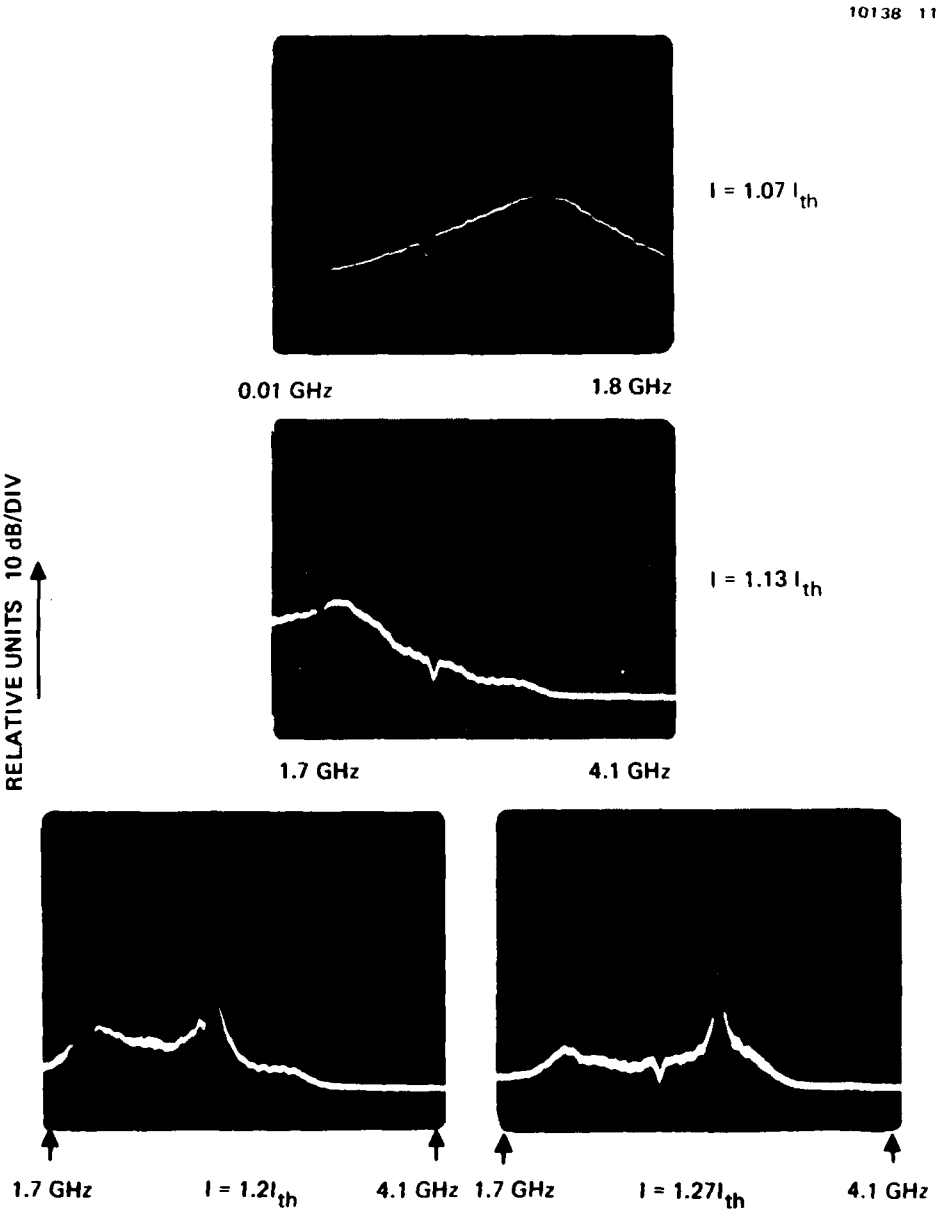

Figure 35. Experimental light output versus frequency for the CSP-SP laser. No external cavity is present.

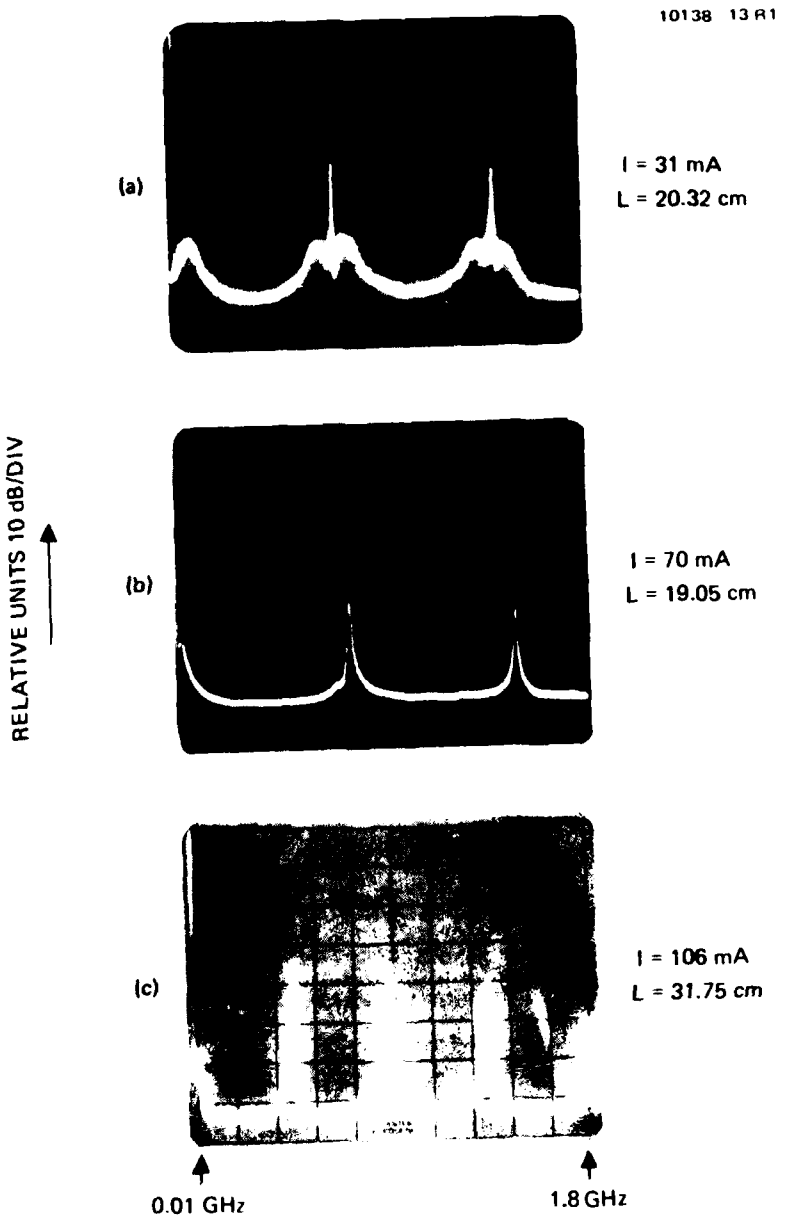

Figure 36. Experimental light output versus frequency plots when an external cavity is aligned with the lasers described in Figures 33 through 35. (a) BH-SP, (b) CSP-SP, (c) G.O.-SP.

megahertz. The pulse outputs for several lasers are shown in Figures 37 and 38. Note that the pulse width is detector limited and the modulation depth is close to 100% for those lasers having a sharp narrow-band noise resonance (Figures 33 and 34). We have obtained efficient mode-locked pulses with frequencies ranging from 400 MHz to 1.2 GHz. The optimum frequency depends on the actual laser structure used.

The amplitude, pulse width, and frequency of the mode-locked pulses depend on several factors. First, assuming that lasers displaying a sharp narrow band noise resonance have a high density of saturable absorbing defects,[25] then it follows from Section 4.B that the process can be described using either the small-signal microwave gain concept or the numerical calculations with saturable electron traps. In either case, pulsations can be induced when: the density of saturable absorbers is high, the optical coupling from the external cavity is above a certain level ($R_f \gtrsim 0.1$), and one of the induced cavity harmonics falls within the positive gain line. We expect the amplitude, pulse width, and frequency of the induced pulsations to vary both with external cavity length and injection current. In lasers where the noise resonance bandwidth is comparatively wider (Figure 35) than the lasers described in Figures 33 and 34, we find broader mode-locked pulses ($\tau_{p_{1/2}} \sim 400$ psec), as shown in Figure 37(a). In strongly self-pulsing lasers with very well defined noise resonances, it is possible to induce pulsations without an external rf signal (shown in Figure 38). Blocking the external cavity quenches the mode-locked pulses, while applying an rf signal at f_c tends to stabilize and possibly narrow the pulses. This result implies a type of passive mode locking and is similar to the observations made by Ippen[15] et al. and Paoli et al.[39] Figure 39 shows the effect of varying the external cavity length and the injection current on the output characteristics of a GO-SP laser. Note the resonant behavior for the amplitude of the pulsations as we vary the injection current (Figure 39). In regions far from the optimum current, the pulse width tends to broaden significantly ($\tau_{p_{1/2}} \gg 400$ psec). Figure 44 shows the effect of varying the length of the external cavity. For lengths greater

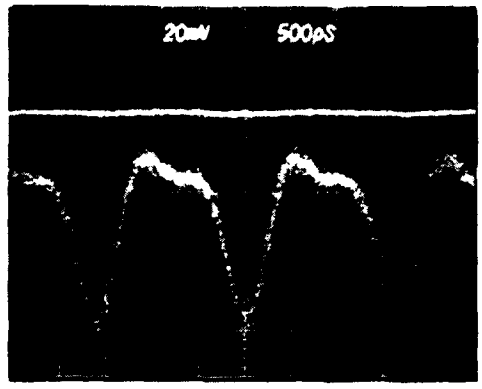

(a)

I = 72 mA
L = 23.5 cm
$\tau_{P_{1/2}}$ = 300 ps

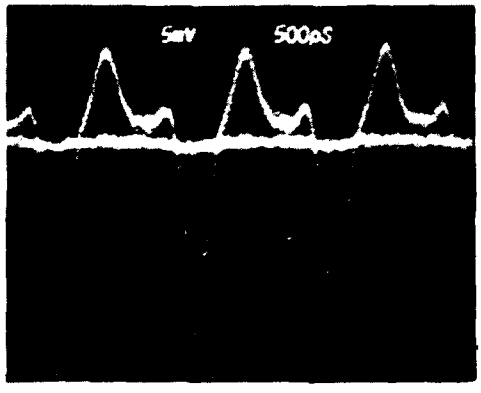

(b)

I = 31 mA
L = 22.9 cm
$\tau_{P_{1/2}} \leq$ 200 ps

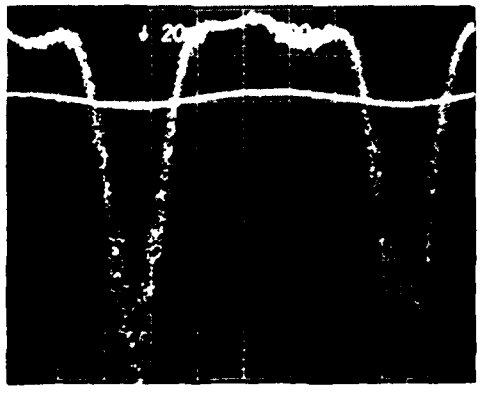

(c)

I = 107 mA
L = 17.15 cm
$\tau_{P_{1/2}} \leq$ 200 ps

Figure 37. Experimental temporal display showing the light output when the lasers described in Figures 33 through 35 are operated in an external cavity and modulated at f_1. (a) CSP-SP, (b) BH-SP, (c) G.O.-SP. (No B&H amplifier was used.)

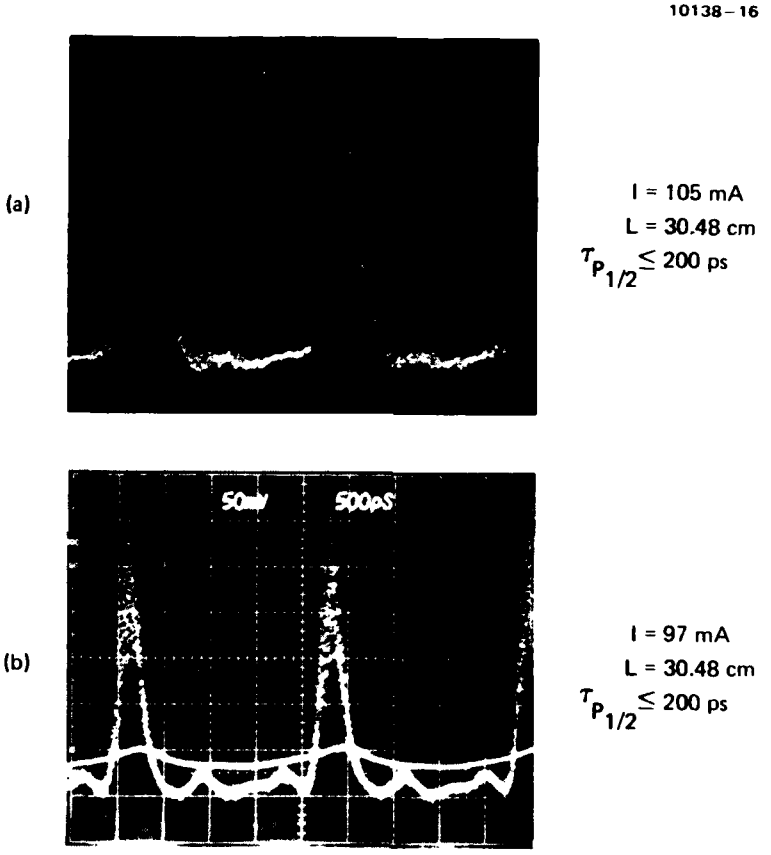

Figure 38. Experimental temporal display showing the light output in a laser with a high density of saturable absorbing defects, and operating in an external cavity. (G.O.-SP). (a) No modulation current applied, (b) with modulation current at f_c.

Figure 39(a). Experimental pulse amplitude versus current. Note the broadening of the pulsewidth from J below 1.03 J_{th} and above 1.1 J_{th}.

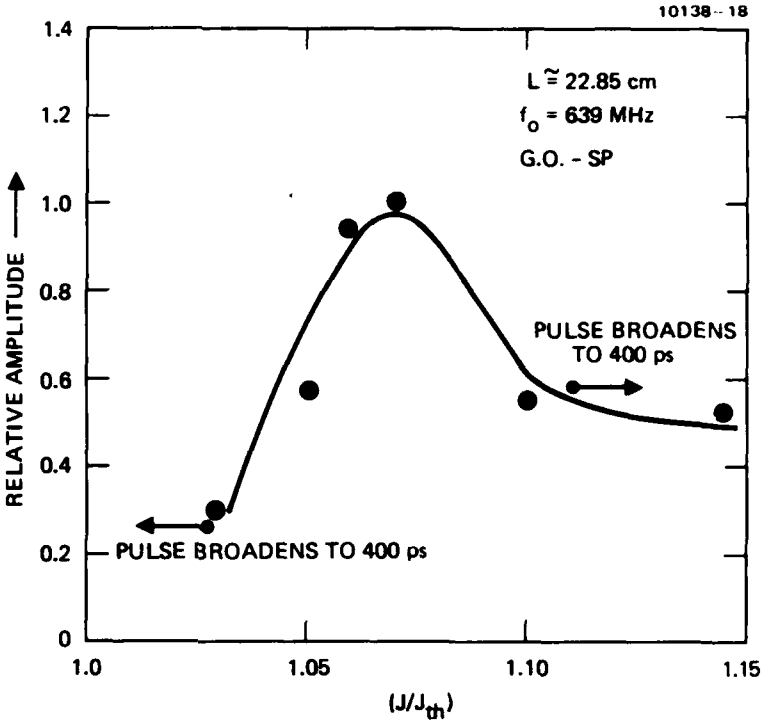

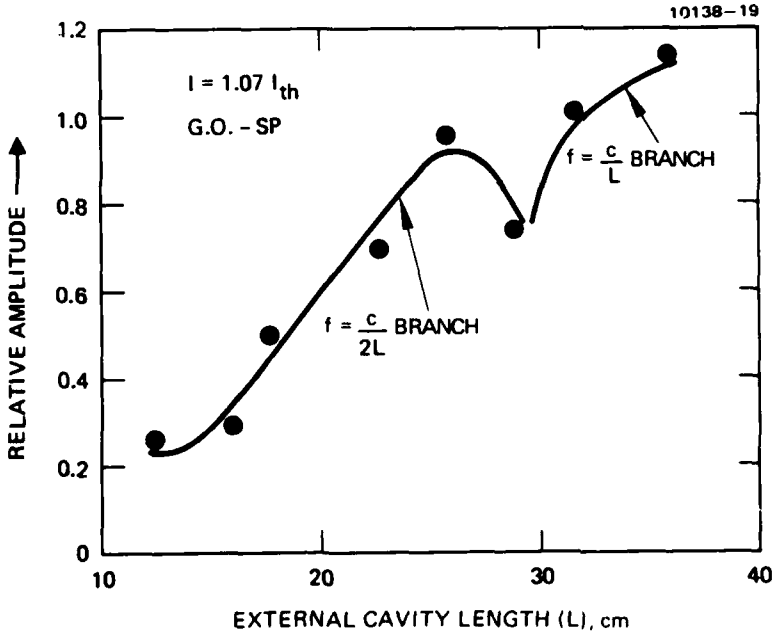

Figure 39(b). Experimental pulse amplitude versus external cavity length. Note that the frequency of the mode-locked pulses is $c_o/2L$ for $L < 30$ cm, while it is c_o/L for $L > 30$ cm.

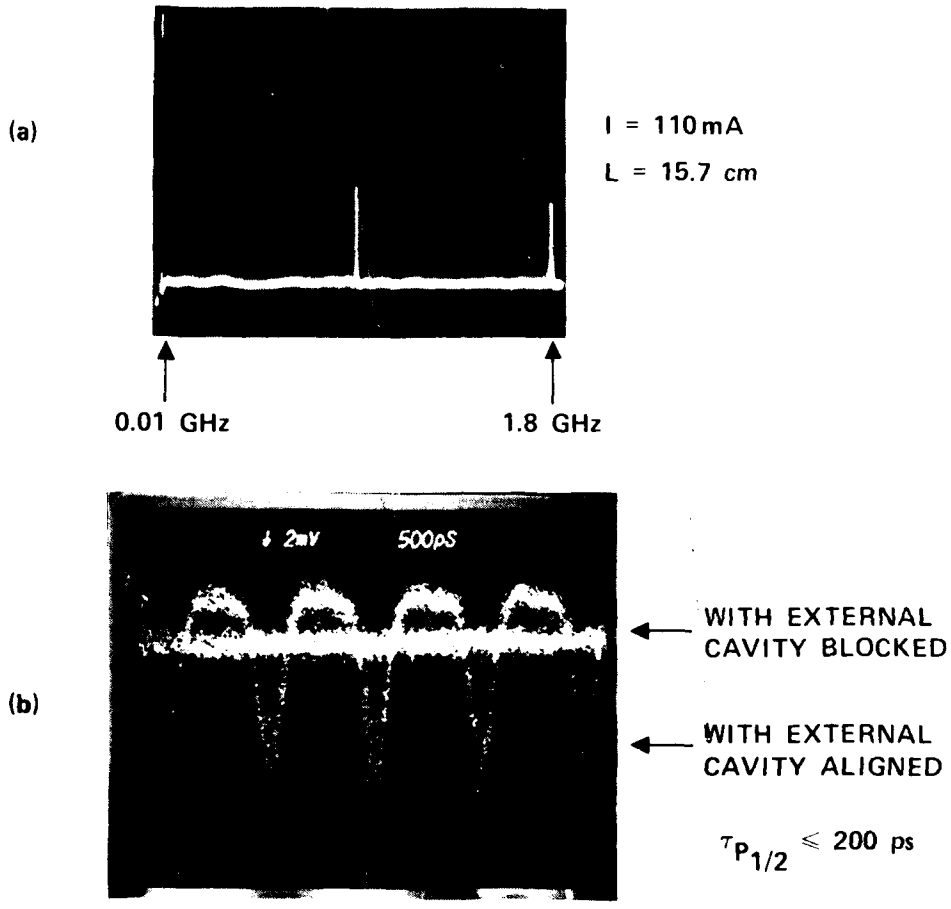

Figure 40. Experimental light output plots for an AR coated laser-external cavity combination. (a) Experimental light output versus frequency with the external cavity aligned. Note the sharp induced resonances. (b) Temporal display when an rf signal with a frequency corresponding to f_c is applied to the laser. The laser used was the same as that described in Figure 33. (No B&H amplifier was used).

than 30 cm, the induced pulsation occurs at the second cavity harmonic (c/L). Comparison of the experimental results (Figures 39 and 40) with the numerical calculations (Figures 27 and 28) shows good agreement. The slight discrepancies for the length where the maximum pulse amplitude occurs can be corrected by assuming a slightly lower electron trap density.

Figure 40 describes the temporal output obtained after we AR-coated one facet (using a sputtered $\lambda/4$ Al_2O_3 film) of the injection laser described in Figure 38. We have been able to obtain detector-limited pulses with $\sim$1 GHz repetition rate for the AR-coated laser-external mirror combination. The bandwidth for the mode-locking was less than 5 MHz. The threshold current of the AR-coated laser increases from 105 mA (no AR coating) to 122 mA (after the AR coating). Using Eqs. 3 through 5 from Ref. 7, we calculate reflectivity of the AR-coated facet to be 4 to 6%. The maximum repetition rate for the mode-locking is apparently limited by the injection laser and not by the external cavity length. Reducing the external cavity length to below 13 cm (f_c = 1.15 GHz) decreases the pulse amplitude at f_c and causes the mode-locking frequency to jump to a lower value ($f \simeq 1/2\ C/2L$). We were also able to increase the external cavity length beyond 32 cm without observing a jump in frequency. However, the pulse amplitude is very unstable beyond this length.

Section 4.B discussed the model used to describe an injection laser with saturable absorbers operating in an external optical cavity. We stated that the model does not include the effects of multilongitudinal modes and the possible coupling between them. To access the possible correlation between the longitudinal modes of the laser and mode locking, we have measured the spectral width of the lasing emission for all the lasers used. These data are summarized in Table 5 (under the longitudinal mode heading). We have observed that only in those lasers having either a narrow-band noise resonance or self-pulsations and also having a relatively wide spectral width ($\Delta\lambda_{1/2} \sim 50\text{Å}$) can we obtain pulses that are detector limited and have 100% modulation depth. We have also observed that "good" mode locking cannot be obtained in lasers having a

narrow-band noise resonance and a narrow spectral width ($\Delta\lambda_{1/2} \sim 10\text{Å}$). In the latter case, the temporal output resembles Figure 37(a), and a significant amount of low frequency noise is present. However, we have also observed that the narrow-band noise frequency f_p occurs in these lasers at a very high value ($f_p > 1$ GHz) and has a very rapid variation with current compared to lasers having a wide spectral width. Furthermore, the amplitude of the noise resonance begins to decrease after a certain drive current. A plot showing the variation of narrow-band noise resonance frequency versus current for the various types of lasers is shown in Figure 41. Note that the variation of f_p with current is quite different for those lasers having a narrow spectral width than for those with a wider spectral width. Several characteristics are worth noting. First, the pulsation frequency is higher for lasers having a narrow spectral width. Second, there is a turning point in the curves where the pulsation frequency changes very rapidly with current. If we assume that all the lasers are identical except for the density of saturable absorbers, then the lasers with the lower pulsation frequency will have a higher density of saturable absorbers.[7,22] This observation suggests that effective mode locking occurs only in lasers having a minimum saturable absorber density. Of course, this minimum depends on the amount of optical coupling from the external cavity, as has been previously calculated.[31,33] Furthermore, the effect of the longitudinal mode coupling in the external cavity is to significantly reduce the pulse width as compared to what would be calculated using the model described in Section 4.B. Ippen et al.[15] recently observed pulses with 5 psec width using an external cavity geometry. However, they observed that the lasers used did not show any self-pulsation. Our observations are not consistent with these results.

Thus far in our discussion, we have not mentioned the temporal stability of the mode-locked pulses. In some of the lasers tested, the mode-locked pulses degrade little over a period of 24 hr, and the alignment of the external cavity can be maintained with minor mirror

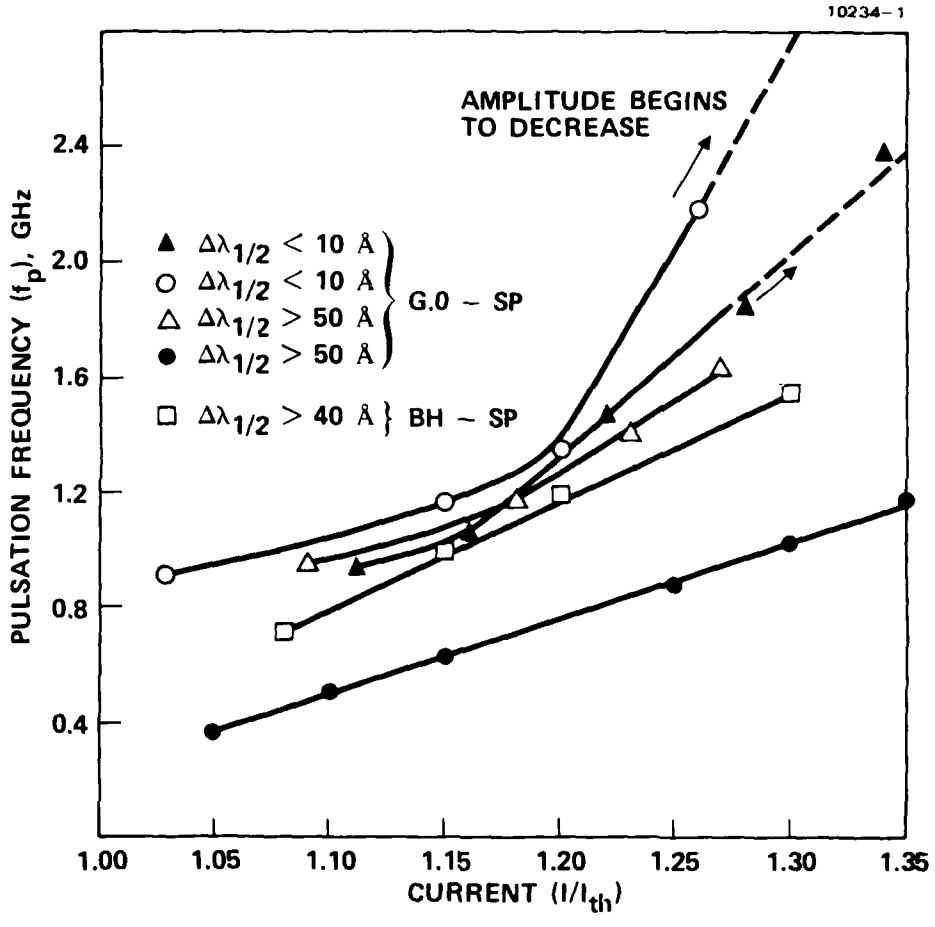

Figure 41. Experimental plot showing the frequency corresponding to the fundamental component of the narrow band noise resonance as a function of dc drive.

adjustments. But in other lasers, the degradation is significant. Increases of 10 to 20% in the threshold current have been observed after operation of a few tens of hours. Also observed have been increases in the low-frequency noise, which makes it increasingly difficult to achieve good rf locking action. In one laser, with detector-limited pulses and 100% modulation depth, the light output degraded rapidly after 1 hr of operation in an external cavity. An examination of the laser facets revealed a blackening of the facet and well-defined cracks, features indicative of catastrophic facet damage. We do not yet understand the cause of this degradation. However, it is worthwhile to point out that the peak powers obtained during mode locking can be very high (0.5 to 1.0 W) and could possibly exceed the power density required for catastrophic facet damage. More work is needed to clarify this point.

E. TIME MULTIPLEXING OF THE LIGHT OUTPUT

Figure 42 shows the experimental arrangement for the multiplexing of the light output. The laser-external geometry has been described in Section 4.A. The multiplexer consists of a pair of prisms and a beam splitter. The light output from the laser is split using the beam splitter and recombined after a suitable time delay Δt. To double the frequency of the light output requires a Δt of $1/2f_c$. Figure 43 shows photographs of the temporal light output before and after the multiplexing. The highest frequency we have obtained after the multiplexing is $\sim$1.7 GHz. We have also examined the light output using a spectrum analyzer and have found that the fundamental frequency at f_c can be suppressed by 40 db by properly controlling the time delay.

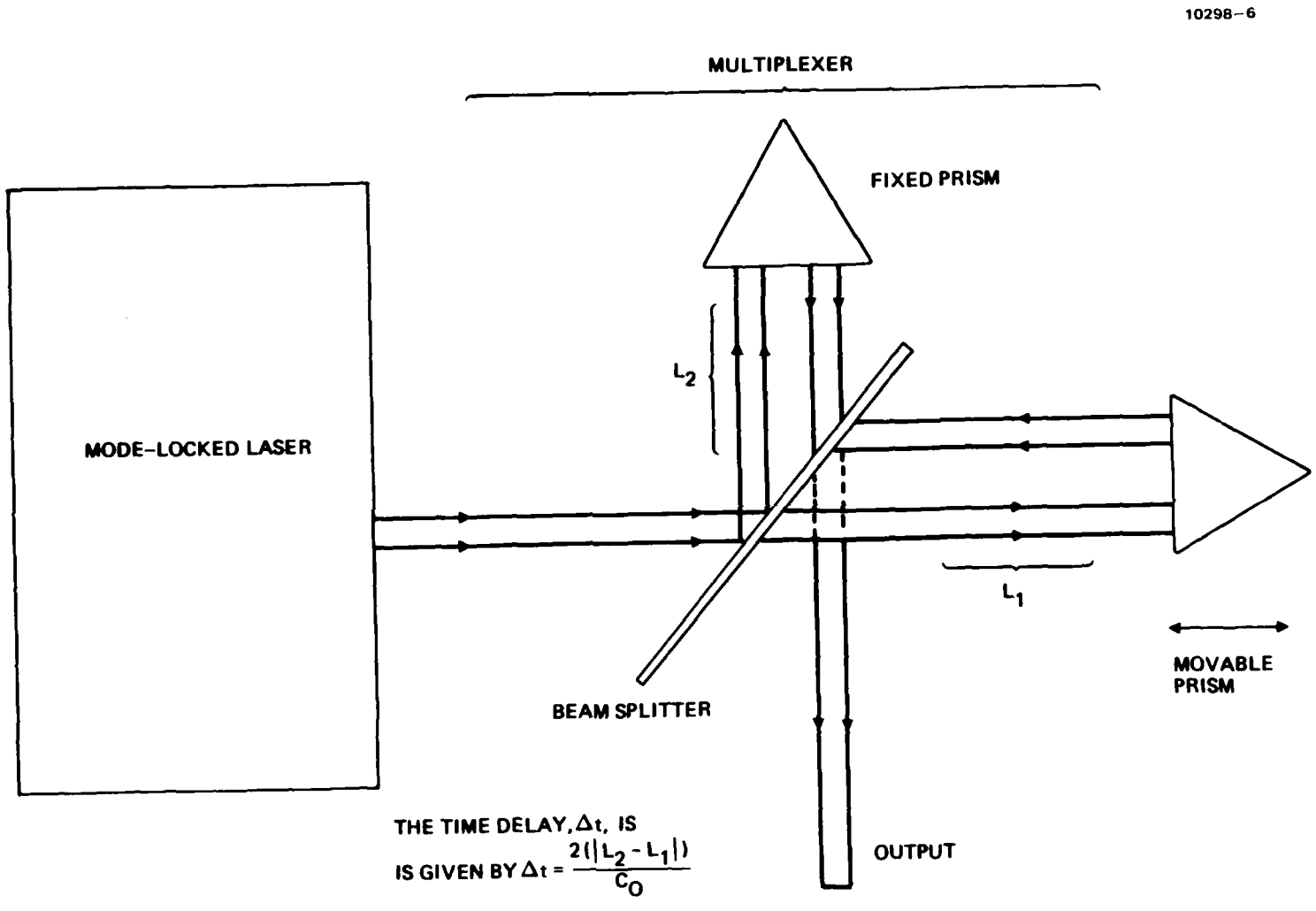

Figure 42. Schematic of the experimental set-up showing a mode-locked laser unit and time multiplexer.

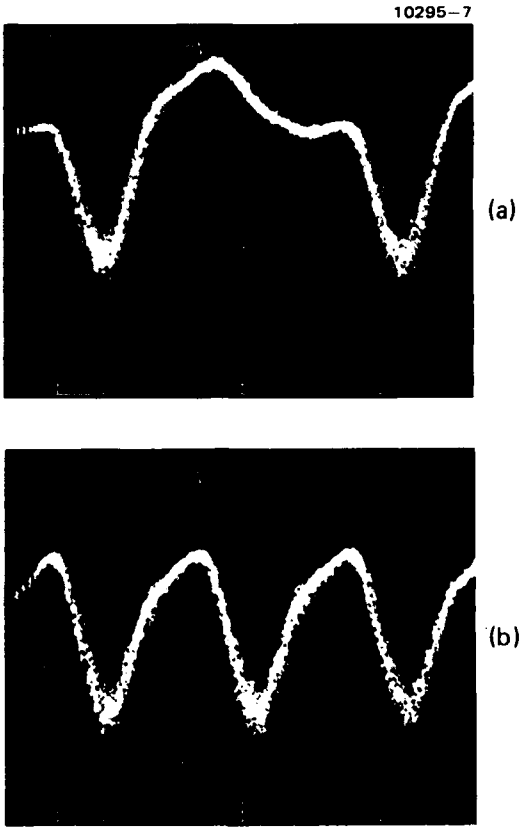

Figure 43. The photographs above display the output versus time from a mode-locked GaAs injection laser. (a) shows the initial light output from the mode-locked laser, (b) shows the light output after frequency doubling has been accomplished. The frequency doubling is performed using a combination of prisms and a beam splitter. The smoothing of the output in (b) is due to the detection system.

SECTION 5

CONCLUSIONS AND FUTURE WORK

This report has discussed our studies of the high-frequency characteristics of (GaAl)As injection lasers, high-speed optical detectors, and mode-locking of (GaAl)As injection lasers. To our knowledge, this represents the first extensive characterization and documentation of these device properties, which are of utmost importance in microwave-optical signal-processing systems.

We found that commercial (GaAl)As injection lasers can only be modulated up to 5 GHz. Therefore, a definite need exists for redesigned laser structures and strip-line circuits to improve the high-frequency performance of these lasers.

In our study of high-speed optical detectors, we concluded that no commercial detector is capable of responding beyond 7 GHz. As a first step towards the realization of a detector that can operate at X-band frequencies, we performed an extensive theoretical and experimental characterization of the GaAs MESFET optical detector. The knowledge obtained in the study of GaAs MESFET detectors will be important in the design of high-speed photoconductive detectors, which are especially suitable for analog signal processing systems.

The study of mode-locking in (GaAl)As injection lasers represents the first thorough experimental and theoretical examination of this process. We concluded that mode-locking in (GaAl)As injection lasers is closely correlated to the ability of a laser to self-pulse. Self-pulsation in (GaAl)As injection lasers has been correlated to either electron traps, or saturable absorbing defects, and thus mode-locking in injection lasers is very similar to passive mode-locking in dye lasers using a saturable absorber with a slow recovery time. We have been able to produce picosecond pulses at gigahertz rates by mode-locking a (GaAl)As injection laser. In other experiments, we time multiplexed the light output from a (GaAl)As mode-locked laser and doubled the frequency (to ≈1.7 GHz). To our knowledge, this represents the first

multiplexing experiments using a mode-locked injection laser operating above 1 GHz.

Since this report is the last quarterly report before the final report under this contract, we can be quite specific as to our future plans. We have acquired an optical rail with suitable attachments to be used for a deliverable mode-locked laser unit. A multiplexer will be placed in a separate box. At present, we are packaging the device using the optical rail to align the optics. Although alignment tolerances are quite stringent, modifications to the rail will allow us to complete the alignment before shipping the device. The mode-locked laser will operate at a frequency of $\sim$1 GHz, and the pulse width will be measured using either an auto-correlator or a high-speed optical detector. We anticipate the pulse width will be less than 100 psec.

REFERENCES

1. H. Kressel and J.K. Butler, Semiconductor Lasers and Heterojunctions, Academic Press (1978).

2. L. Figueroa, C.W. Slayman, and H.W. Yen, "Optical-Microwave Interactions in Semiconductor Devices," Hughes Technical Report under contract N00173-77-C-0156 (1980).

3. J.C. Gammel and J.M. Ballantyne, IEDM Technical Digest, 120 (1978).

4. K. Jarasiunas, C. Hoffman, H. Gerritsen, and A. Nurmikku, in Picosecond Phenomena, edited by C.V. Shank et al., 327 (1978).

5. S. Wang, Solid State Electronics, McGraw Hill (1966).

6. E. Mohn, "Symposium on GaAs, paper 17 (1968).

7. L. Figueroa, K. Lau, H.W. Yen, and A. Yariv, J. Appl. Phys. V 51, 3062 (1980).

8. R.P. Salathe, Appl. Phys. V. 20, 1 (1979).

9. R.F. Broom, E. Mohn, C. Risch, and R. Salathe, IEEE J. Quantum Electron. V. QE-6, 328 (1970).

10. T.L. Paoli and J.E. Ripper, IEEE J. Quant. Elect. V. QE-6, 335 (1970).

11. T.L. Paoli, J.E. Ripper, A.C. Morosini, and N.B. Patel, IEEE J. Quantum Electron. V. QE-11, 525 (1975).

12. P.T. Ho, L.A. Glasser, E.P. Ippen, and H.A. Haus, Appl. Phys. Lett. V. 33, 241 (1978).

13. L.A. Glasser, Electron. Lett. V. 14, 725 (1978).

14. P.T. Ho, Electron. Lett. V. 15, 527 (1979).

15. E.P. Ippen, D.J. Eilenberger, and R.W. Dixon, Appl. Phys. Lett. V. 37, 267 (1980).

16. M.B. Holbrook, W.E. Sleat, and D.J. Bradley, Appl. Phys. Lett. V. 37, 59 (1980).

17. J.P. Van der Ziel and R.M. Mikulyak, J. Appl. Phys. V. 51, 3033 (1980).

18. H. Ito, H. Yokoyama, and H. Inaba, Electron. Lett. V. 16, 620 (1980).

19. N.G. Basov, IEEE J. Quantum Electron. V. QE-4, 855 (1968).

20. T. P. Lee and R. H. R. Roldan, IEEE J. Quant. Elect., V. QE-6, 339 (1970)

21. D. Kato, Appl. Phys. Lett., V. 31,588 (1977)

22. J. A. Copeland, Elect. Lett., V. 14, 809 (1978)

23. R. W. Dixon and W. B. Joyce, IEEE J. Quant. Elect., V. QE-15, 470 (1979)

24. J. P. Van der Ziel, J. L. Merz, and T. L. Paoli, J. Appl. Phys., V. 50,4620 (1979)

25. B. W. Hakki, "Instabilities in output of injection lasers," J. Appl. Phys., V. 50, 5630 (1979)

26. T. L. Paoli and J. E. Ripper, Phys. Rev. Lett., V. 22, 1088 (1969)

27. L. W. Casperson, IEEE J. Quant. Elect., V. QE-14, 756 (1978)

28. R. L. Hartman, R. A. Logan, L. A. Koszi, and W. T. Tsang, J. Appl. Phys., V. 40,4616 (1979)

29. F. R. Nash, R. L. Hartman, T. L. Paoli and R. W. Dixon, presented at the Int. Devices Meeting, Washington D. C., paper 5.4, (1979)

30. K. Mitsuishi, N. Chinone, H. Sato, and K. Aiki, IEEE J. Quant. Elect., V. QE-16, 728 (1980)

31. L. Figueroa, K. Lau, and A. Yariv, Appl. Phys. Lett., V. 36, 248 (1980)

32. K. Lau, L. Figueroa, and A. Yariv, to be published in IEEE J. Quant. Elect. (Dec. 1980).

33. G. H. C. New, IEEE J. Quant. elect, V. QE-10, 115 (1975)

34. H. Haus, IEEE J. Quant. Elect, V. QE-11, 736 (1975)

35. B. W. Hakki, J. Appl. Phys., V. 51, 68 (1980)

36. H. W. Yen, and M. K. Barnoski, "Optical Microwave Interactions in Semiconductors," Hughes Technical Report under contract N00173-77-C-0156 (1978)

37. T. L. Paoli, IEEE J. Quant. Elect, V. QE-13, 314 (1977)

38. G. Arnold, and K. Peterman, Appl. Phys. V. 10, 311 (1978)